A limited area model (LAM) intercomparison study of a TWP-ICE active monsoon mesoscale convective event

Ping Zhu,[1] Jim Dudhia,[2] Paul R. Field,[3] Kathrin Wapler,[4] Ann Fridlind,[5] Adam Varble,[6] Ed Zipser,[6] Jon Petch,[3] Ming Chen,[2] and Zhenduo Zhu[1]

Received 21 June 2011; revised 25 April 2012; accepted 26 April 2012; published 6 June 2012.

[1] A limited area model (LAM) intercomparison study is conducted based on a tropical monsoonal deep convection case observed during the Tropical Warm Pool - International Cloud Experiment (TWP-ICE). The LAM simulations are compared with the variational analyses (VA) based on the Atmospheric Radiation Measurement (ARM) observations and the cloud resolving model (CRM) simulations forced by the VA. Driven by the ECMWF analyses or global model forecasts, LAMs are able to produce the large-scale thermodynamic field reasonably well compared with the VA. However, the LAM simulated dynamic fields, such as the large-scale horizontal divergence, vertical velocity, and cyclogenesis in the monsoonal trough, have a large inter-model spread and deviate substantially from observations. Despite the differences in large-scale forcing, there is certain consistency between the CRM and LAM simulations: stratiform ($w \leq 1$ m s^{-1}) ice clouds dominate the cloud fraction and convective ($w > 3$ m s^{-1}) clouds occupy less than 3 percent of the total cloudy area. But the hydrometeor content of stratiform ice clouds is only one tenth of that of convective and transitional (1 m s^{-1} $< w \leq 3$ m s^{-1}) ice clouds. However, there is a large inter-LAM spread in the simulated cloud fraction and hydrometeor mixing ratios. The inter-LAM difference in solid phase hydrometeors (cloud ice, snow, and graupel) can be up to nearly a factor of 10. Among all the hydrometeor types, the stratiform ice clouds are simulated least consistently by the LAMs. The large inter-LAM spread suggests that obtaining consistent and reliable dynamic and cloud fields remains a challenge for the LAM approach.

Citation: Zhu, P., J. Dudhia, P. R. Field, K. Wapler, A. Fridlind, A. Varble, E. Zipser, J. Petch, M. Chen, and Z. Zhu (2012), A limited area model (LAM) intercomparison study of a TWP-ICE active monsoon mesoscale convective event, *J. Geophys. Res.*, *117*, D11208, doi:10.1029/2011JD016447.

1. Introduction

[2] Deep convection in the western tropical Pacific is the primary mechanism for driving planetary circulations, such as the Hadley and Walker circulations, and intraseasonal variabilities, such as Madden-Julian Oscillation (MJO) [e.g., *Del Genio and Yao*, 1988; *Del Genio and Kovari*, 2002; *Yang and Slingo*, 2001]. Despite its importance in the climate system, the representation of convection in general circulation models (GCMs) remains a great challenge in climate simulations and projections [e.g., *Arakawa*, 2004; *Randall et al.*, 2003, 2007].

[3] To facilitate our understanding of the structure and evolution of tropical deep convection, the resulting cirrus clouds, the induced convective transport, and their impact on the large-scale dynamics and thermodynamics, the Atmospheric Radiation Measurement (ARM), GEWEX Cloud Systems Study (GCSS), and Stratospheric Processes And their Role in Climate (SPARC) programs organized a joint model intercomparison study based on the Tropical Warm Pool - International Cloud Experiment (TWP-ICE). TWP-ICE took place over Darwin, Australia from January 20 through February 12, 2006 [*May et al.*, 2008]. During this period, Darwin experienced a dramatic weather change associated with the Australian monsoon [*Drosdowsky*, 1996] shifting from an initial active monsoon period, to a suppressed monsoon period, and finally to a monsoon break period. The wide variety of convective activities observed during TWP-ICE provides a good opportunity to evaluate the ability of various types of numerical models to reproduce the observed cloud systems associated with the monsoon.

[1]Department of Earth and Environment, Florida International University, Miami, Florida, USA.
[2]Mesoscale and Microscale Meteorology, National Center for Atmospheric Research, Boulder, Colorado, USA.
[3]Met Office, Exeter, UK.
[4]Deutscher Wetterdienst, Offenbach, Germany.
[5]NASA Goddard Institute for Space Studies, New York, New York, USA.
[6]Department of Atmospheric Sciences, University of Utah, Salt Lake City, Utah, USA.

Corresponding author: P. Zhu, Department of Earth and Environment, Florida International University, MARC 360, 11200 SW 8th St., Miami, FL 33199, USA. (zhup@fiu.edu)

0148-0227/12/2011JD016447

The TWP-ICE model intercomparison study consists of four components: intercomparisons of global numerical weather prediction (NWP) models, cloud resolving models (CRMs), single column models (SCMs), and limited area models (LAMs). This paper reports the LAM intercomparison study of the strongest active monsoonal convective event observed during the TWP-ICE campaign.

[4] Since convection is not resolved in large-scale models and only select information can be obtained from observations, CRMs have been serving as a major numerical tool for investigating cloud dynamic and thermodynamic processes, including evaluating and improving cloud and convection parameterizations. Over the past few decades, the CRM approach has greatly advanced our understanding of convection over a spectrum of scales. Recently, *Randall et al.*'s [2003] super parameterization concept further illustrated that CRMs can act within large-scale models to provide sub-grid structures. CRMs are still limited, however, since they are initialized with idealized vertical profiles, forced by horizontally homogeneous large-scale and surface forcings, and supplied with periodic lateral boundary conditions. Such a numerical strategy is adequate for simulating maritime convection in undisturbed conditions, but may not be appropriate for inhomogeneous surface conditions or inhomogeneous large-scale forcings. In such situations, variations at the inflow boundaries can be substantially different from those at the outflow boundaries. Currently, the question still remains as to the extent that the numerical approach used by CRMs can affect the fidelity of simulated convection when horizontal heterogeneity is substantial. On the other hand, NWP models are initialized with global analysis/reanalysis or global forecast data and avoid the lateral boundary condition issues of CRMs, but the resolution of global models typically is too low to resolve cloud/convection processes. The deficiencies of CRMs and NWP models are largely overcome by high resolution LAM (or regional model) simulations in which the initial and lateral boundary conditions are provided by global analyses/reanalyses or global forecasts, the same forcing data that are used to drive NWP models. Ever increasing computational power has allowed LAMs to be executed at equivalent resolutions to CRMs, or even large-eddy simulations (LESs) in some cases, through use of downscaling techniques to explicitly resolve cloud moist processes. In this regard, LAMs may be considered to be a numerical approach that bridges the gap between CRMs and coarser resolution NWP models.

[5] Although recent successes [e.g., *Kain et al.*, 2006; *Weisman et al.*, 2008; *Zhu et al.*, 2010] in high resolution LAM simulations have demonstrated the potential of this approach in convection and cloud simulations, the LAM approach requires extensive evaluations for different cloud systems in various climate regimes. Unlike CRMs in which the initial profiles and large-scale forcings are prescribed, LAMs are forced through updating their lateral boundary conditions provided by either global analyses/reanalyses or forecasts. Since LAMs use nests to gradually scale down to cloud resolving scale, the dynamic and thermodynamic fields simulated by LAMs may differ from the large-scale forcings provided by the global data depending on the processes resolved by nested domains. In two-way nested LAM simulations, the large-scale dynamic and thermodynamic fields may change due to the upscale feedbacks from the resolved cloud/convection processes. When one-way nestings are applied, although the upscale feedback is not supported, the down-scaling impact on the LAM cloud resolving simulation through nests can still be significant due to the mesoscale processes resolved by the nests. Thus, in addition to evaluating whether robust convection and clouds can be generated under certain large-scale dynamic and thermodynamic forcing (a major focus of CRMs), it is also important to examine whether LAMs can realistically simulate the large-scale forcings derived from observations.

[6] The land-ocean contrast at Darwin coupled with the complicated synoptic features and mesoscale convective systems (MCSs) associated with the Australian monsoon provides a good opportunity to test and evaluate the LAM's capability to reproduce the observed convection in highly inhomogeneous conditions. Although there have been individual efforts in simulating TWP-ICE convection using the cloud resolving Weather Research and Forecasting (WRF) model [e.g., *Wang et al.*, 2009; *Wapler et al.*, 2010], the robustness of state-of-the-art regional models in simulating convective systems at the cloud resolving scale has yet to be extensively evaluated. Hence, considering the great success of past CRM, LES, and SCM intercomparison studies organized by the GCSS cloud working groups, the ARM/GCSS/SPARC initiated its very first LAM intercomparison study as a unique component of this joint modeling study on tropical deep convective clouds. The LAM intercomparison presented here focuses on issues that may not be appropriately addressed by the accompanying CRM, SCM, and NWP intercomparison studies. In particular, we address following two questions: (1) Can LAM simulations capture the observed wide range of dynamical processes during a significant TWP-ICE mesoscale convective event in the active monsoon period? (2) Can LAMs statistically produce similar cloud structure to those simulated by CRMs if LAMs are configured with the same resolution as that of CRMs?

[7] This paper is organized as follows. Section 2 provides a description of the case setup and configurations of the participating models. The results of model intercomparison are presented in section 3. Finally, a summary and discussion are provided in section 4.

2. Simulation Setup

2.1. Case Specification

[8] During the TWP-ICE field campaign, Darwin experienced different monsoon phases. Although several numerical runs were proposed for LAMs to simulate the different phases of monsoon, in this paper we only focus on the LAM intercomparison of the active monsoon period from 12:00 UTC January 22 to 00:00 UTC January 26, which includes the strongest observed deep convective event (around 19 UTC January 23, 2006) named as Event C by *Fridlind et al.* [2010] and *Xie et al.* [2010a]. The results for the other periods will be reported in a separate paper.

2.2. Participating Models

[9] Three LAMs, namely, WRF, the Met Office's Unified Model (MOUM), and the COnsortium for Small-scale MOdeling (COSMO) participated in this LAM intercomparison study. In this study, WRF Version 3.1.1 was used to simulate TWP-ICE convection. The major model physical

Table 1. Major Model Configurations for Participating LAMs[a]

LAM	WRF-1	WRF-2	WRF-3	WRF-4	MOUM	COSMO
Innermost domain grids	450 × 330	450 × 330	450 × 330	438 × 333	414 × 310	160 × 119
Grid spacing	1 km	1 km	1 km	1 km	1 km	2.8 km
Vertical levels	92(15)	92(15)	92(15)	76(13)	70(24)	50(16)
Nesting	two-way	two-way	two-way	two-way	one-way	one-way
Microphysics	Thompson	WSM6	Morrison 2-mom	WSM6	Mixed phase	Kessler 6-class
	Q_c, Q_r	Q_c, Q_r	Q_c, Q_r	Q_c, Q_r	Q_c, Q_r	Q_c, Q_r
	Q_i, Q_s, Q_g	Q_i, Q_s, Q_g	Q_i, Q_s, Q_g	Q_i, Q_s, Q_g	Q_i	Q_i, Q_s, Q_g
Land surface model	Thermal diffusion	Thermal diffusion	Thermal diffusion	Noah	MOSES	Heise & Schrodin
PBL	YSU	YSU	YSU	YSU	Lock	MY-2.5
Forcing data	ECMWF	ECMWF	ECMWF	ECMWF	ECMWF	GME

[a]Vertical levels in parentheses indicate the levels below 2 km.

schemes include the Yonsei University boundary layer scheme (YSU) [*Noh et al.*, 2003], the Rapid Radiative Transfer Model (RRTM) [*Mlawer et al.*, 1997] for longwave radiation, the *Dudhia* [1989] scheme for shortwave radiation, and the Kain-Fritsch [*Kain and Fritsch*, 1993] scheme for deep convection activated in the coarse WRF domains (see below). These schemes were kept the same in all WRF simulations. To test the sensitivity of simulated TWP-ICE convection to model vertical resolution, land surface processes, and cloud microphysics, four different configurations of WRF were used in this study. Table 1 summarizes the major differences of these configurations. In the first three WRF configurations (named as WRF-1, WRF-2, and WRF-3 hereafter), there are 92 vertical levels in which 15 levels are below 2 km. These three WRF configurations are exactly the same except for the microphysical scheme. WRF-1, WRF-2, and WRF-3 use Thompson [*Thompson et al.*, 2008], WSM 6-class [*Hong and Lim*, 2006], and Morrison 2-moment [*Morrison et al.*, 2009] microphysical schemes, respectively. In these three runs, the non-hydrostatic atmospheric model is coupled to a simple 5-layer thermal diffusion land surface model. Like WRF-2, WRF-4 uses the WSM 6-class microphysical scheme, but it only has 76 vertical levels in which 13 levels are below 2 km. In this run, the non-hydrostatic atmospheric model is coupled to the Noah land-surface model [*Chen and Dudhia*, 2001].

[10] Figure 1a shows the TWP-ICE pentagonal sounding array, which covers an area approximately 176 km × 176 km (see *Varble et al.* [2011] for details). The LAM research domain is configured to cover the entire pentagonal experimental area. Figure 1b shows the model domain configuration used by WRF simulations. The innermost domain, D4, centered at 130.891°E, 12.425°S with a grid spacing of 1 km, covers an area of 450 km × 330 km. The land fraction of the innermost LAM research domain is about 57.9%. The 1 km horizontal resolution of LAMs is the same as that of accompanying CRMs, which cover an area approximately equivalent to the pentagonal experimental area. Therefore, to make an appropriate comparison with observations and CRM simulations, the analyses of LAM simulations were made over the pentagonal experimental area. Using the same subset of LAM's innermost domain for analyses also minimizes the possible effect of the different domain size used by the participating LAMs. Moreover, since the pentagonal area is far away from the lateral boundaries, the lateral boundary influence on model analyses can be minimized. As illustrated by Figure 1b, to scale down to 1 km resolution, three two-way nests with the nesting ratio 1:3 are used. One of the purposes of using nests is to provide the innermost cloud-resolving domain an appropriate mesoscale forcing produced by outer domains. Technically, either two-way or one-way nesting can fulfill this task. The advantage of two-way nesting is to obtain an upscale feedback as we discussed previously, which, to some extent, may affect the resolved mesoscale forcing. To examine if the nesting methods will affect the results for this case, we performed a sensitivity test of WRF-1 with one-way nesting. The statistics of the innermost domain simulation are almost identical to that of baseline WRF-1. Thus, we believe the choice of nesting type will not substantially change the statistical results from the innermost cloud resolving domain, at least for this TWP-ICE case. During the simulation, the deep convection scheme is activated in WRF domains D1 (27 km grid spacing) and D2 (9 km grid spacing), but not in D3 (3 km grid spacing) and D4 (1 km grid spacing).

[11] The MOUM is a non-hydrostatic model that uses a semi-Lagrangian advection scheme [*Cullen et al.*, 1997; *Davies et al.*, 2005]. The major model physical parameterizations include: the Lock boundary layer scheme [*Lock et al.*, 2000], a mixed phase cloud microphysics [*Wilson and Ballard*, 1999] but without separation between ice, snow, and graupel, the Met Office Surface Exchange Scheme (MOSES) land surface model [*Essery et al.*, 2003], a convection scheme [*Gregory and Rowntree*, 1990], and a subgrid cloud representation [*Smith*, 1990]. MOUM uses a one-way nesting technique to scale down from global simulation through 12 km, to 4 km grids and finally to 1 km resolution. The convection scheme is active for grids coarser than the 1 km innermost grid. For this study there are 70 vertical levels with 24 levels below 2 km.

[12] COSMO is a fully compressible and non-hydrostatic model. The major model physics include: a level-2.5 turbulent mixing scheme [*Mellor and Yamada*, 1974]; Louis surface layer parameterization [*Louis*, 1979], a two-stream radiation scheme [*Ritter and Geleyn*, 1992] allowing for full cloud-radiation feedback, the Tiedtke mass flux convection scheme [*Tiedtke*, 1989], and a Kessler-type grid-scale precipitation scheme with parameterized 6 class cloud microphysics. The atmospheric model of COSMO is coupled to a 7-layer soil model [*Heise and Schrodin*, 2002] including a simple vegetation parameterization. Unlike WRF and MOUM, COSMO uses a coarser grid spacing of 2.8 km for the finest domain that has a grid mesh of 160 × 119 with a total 50 vertical levels in which 16 levels below 2 km. The question whether the low resolution used by COSMO will substantially affect the results is left for future study.

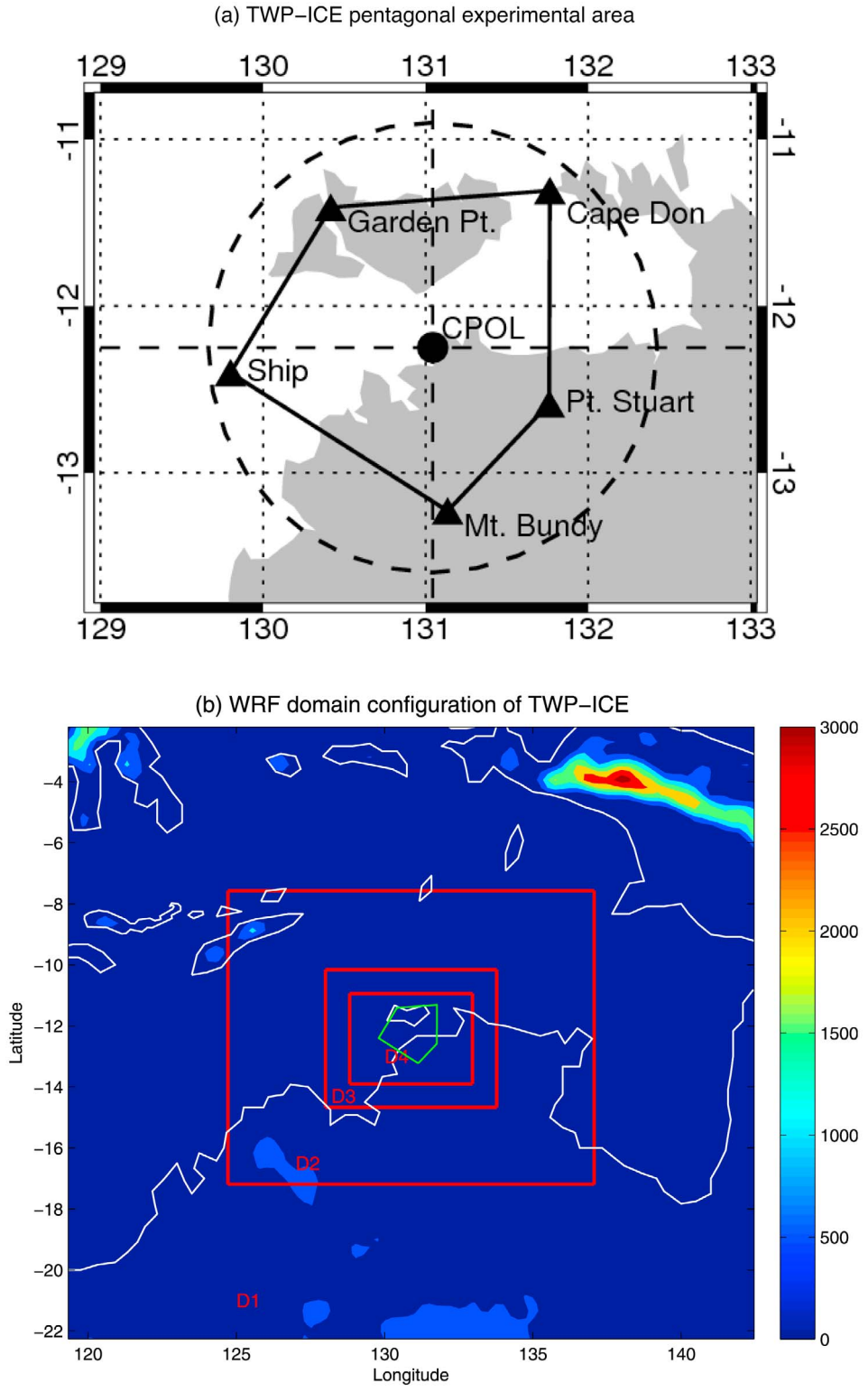

Figure 1. (a) TWP-ICE pentagonal experimental area [after *Varble et al.*, 2011]. (b) Multiple nested WRF domain configuration centered at 130.891°E and 12.425°S. The background shades indicate the terrain height. Coastlines are indicated by the white curves. The enclosed green lines indicate the pentagonal experimental area. D1, D2, D3, and D4 indicate the parent domain and the two-way nested Domains, respectively.

2.3. LAM Forcing Strategy

[13] In this study, the high resolution LAM simulations performed by WRF, MOUM, and COSMO are initialized and forced using different strategies. In all WRF simulations, the parent domain (D1) is initialized and driven by the European Centre for Medium-Range Weather Forecasts (ECMWF) analyses. The lateral boundary conditions of WRF domain D1 are updated from the ECMWF analyses every six hours. In the WRF-1, WRF-2, and WRF-3 simulations, the horizontal winds, temperature, and water vapor mixing ratio of ECMWF analyses were nudged in domains D1, D2, and D3 at a nudging coefficient of 0.0003 s^{-1} at all height levels. This prevents the lateral boundary conditions for the LAM research domain D4 from drifting away from the ECMWF analyses. D4 is not nudged and is solely forced through updating its lateral boundary conditions every six hours. But nudging in the outer domains was not used in the WRF-4 simulation. Unlike WRF, the LAM simulation of MOUM is not directly forced by the ECMWF analyses. Instead, the ECMWF analyses are used to initialize the MOUM global model (with resolution of $0.56^\circ \times 0.37^\circ$) every 24 hours at 00:00 UTC. The MOUM global simulation is then used to provide lateral boundary conditions for MOUM LAM simulation. In this sense, the MOUM global model is equivalent to the parent domain D1 in WRF simulations. The lateral boundary conditions of the MOUM 12-km resolution domain are updated every hour from the MOUM global simulation. Likewise, the 12-km resolution simulation is used to force the 4-km resolution simulation, which then is used to force the 1-km resolution simulation through updating lateral boundary conditions every hour. In the COSMO simulation, the 2.8-km resolution domain is driven by a coarse COSMO simulation at a lower resolution (7 km grid spacing, 40 levels), which was nested in the global model (GME) [*Majewski et al.*, 2002] simulation (40 km grid spacing, 40 levels). Table 1 summaries the major differences among WRF, MOUM, and COSMO.

3. Results

[14] Due to the nesting down technique used in the LAM simulations, the simulated dynamic and thermodynamic fields may differ from those in the global forcing data that drive LAM simulations. Thus, to evaluate the capability of LAMs to simulate the clouds associated with the TWP-ICE active monsoonal deep convective event and make a meaningful cloud-scale comparison among different LAMs and the accompanying CRM simulations, it is important to examine whether LAMs can realistically reproduce the observed large-scale dynamic and thermodynamic fields and the resulting cloud and precipitation fields.

3.1. Large-Scale Thermodynamic Fields

[15] Figures 2a and 2b compare the LAM simulated vertical profiles of relative humidity and potential temperature (θ) averaged over the pentagonal area from 00:00 UTC January 23 to 12:00 UTC January 25 with the TWP-ICE variational analyses (VA) derived from the ARM observations [*Xie et al.*, 2010a] and the mean from a subset of CRMs participating in the accompanying CRM intercomparison study. This subset includes seven baseline CRM simulations from *Varble et al.* [2011]. For detailed information of CRMs, please refer to *Fridlind et al.* [2012] and *Varble et al.* [2011]. The results shown here are derived from model 3-D output with time interval of 3 hours. This is the same for other analyses shown later unless otherwise specified. LAMs appear to reproduce the vertical thermodynamic structure reasonably well compared with the VA. In particular, the LAM simulated vertical profiles of potential temperature are consistent with those of VA and CRMs. The normalized profiles show that the spread of simulated θ with respect to VA are less than 0.5% below 15 km. Larger inter-LAM spread is seen at altitudes above 15 km, but the values remain below 2%.

[16] A relatively large model spread is shown in the relative humidity profiles, which may be partially due to the fact that it combines errors in both temperature and moisture. As expected, the relative humidity profile of CRM mean tracks the VA consistently well throughout the entire troposphere. This high degree of consistency results from CRM's special initialization approach and prescribed large-scale forcings. A relatively large spread in relative humidity, however, is seen in the LAM simulations, particularly in the upper troposphere. The mean standard deviation of LAM simulated relative humidity between 10–18 km is 9.4%. WRF-2 and WRF-4 (the two runs that use WSM 6-class microphysical scheme) under-estimate the relative humidity by 10–15 % in the upper troposphere (10–20 km) compared with the VA and other simulations. Since WRF-2 is configured exactly the same as WRF-1 and WRF-3 except for cloud microphysics, this result indicates that the parameterization of subgrid-scale (SGS) processes (cloud microphysics in this case) does have a non-negligible impact on large-scale thermodynamic fields in LAM simulations. Despite the relatively large spread in relative humidity in the upper troposphere, the simulated relative humidities below 10 km are slightly drier, but within the spread of the VA. The mean standard deviation of LAM simulated relative humidity between 0–10 km is only 2.7%. This result along with the well simulated θ profile suggests two things. First, although the impact of resolved processes on large-scale thermodynamic fields is evident in LAM simulations, the large-scale forcing data does provide the first-order approximation of large-scale thermodynamic fields. The similar large-scale thermodynamic fields in LAMs and CRMs makes it possible to compare the simulated cloud fields from the two different numerical approaches (shown later in section 3.4.) Second, although different large-scale forcing data are used in this study to force LAMs, both ECMWF analyses and GME forecasts are able to provide sufficiently accurate large-scale vertical thermodynamic structure in the active monsoonal period compared with the VA, suggesting that both data sets are adequate to drive high resolution LAM simulations for the study of tropical deep convection.

3.2. Large-Scale Dynamic Fields

[17] The LAM simulated vertical profiles of horizontal wind components averaged over the pentagonal area from 00:00 UTC January 23 to 12:00 UTC January 25 are shown in Figures 2c and 2d. The mean horizontal wind profiles are fairly consistent with each other and track those of VA and CRMs fairly well. The standard deviations of LAM mean profiles for U and V component averaged over 0–25 km are only 1.3 m s^{-1} and 1.0 m s^{-1}, respectively. However, as

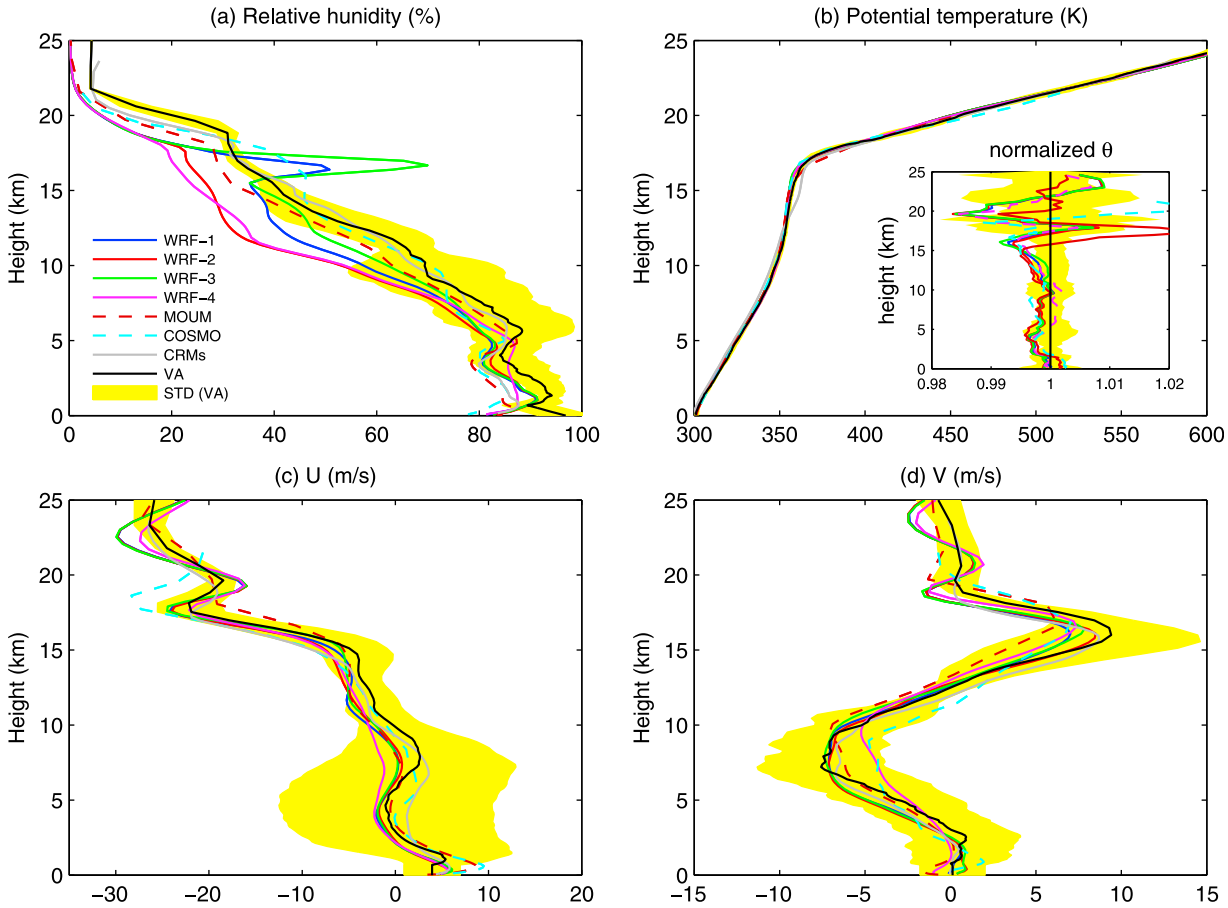

Figure 2. Vertical profiles of LAM simulated (a) relative humidity, (b) potential temperature, and (c and d) horizontal wind components averaged over the pentagonal area from 00:00 UTC January 23 to 12:00 UTC January 25, 2006 compared with those from CRMs and the ARM variational analyses (VA). Yellow shades indicate the standard deviations of VA over the period. The inlaid panel in Figure 2b shows the potential temperature profiles normalized by the mean of VA.

shown in the figures, the standard deviations of VA wind profiles in the period from 00:00 UTC January 23 to 12:00 UTC January 25 are very large in the lower troposphere, which suggests a dramatic change in horizontal wind fields during the active monsoonal period. The large wind direction change of this case was confirmed by a recent study [*Wapler et al.*, 2010]. The large change in wind direction reflects the complicated dynamics during the active monsoonal period. One of the important dynamic features associated with the monsoonal trough is the cyclone development in the low troposphere. As an illustration of the cyclone, Figure 3 shows the instantaneous 2 km high horizontal wind vectors and hydrometeor mixing ratio at 01:00 UTC on January 24 from different LAM simulations. The wind vectors clearly reveal the closed cyclonic flow that covers the entire Darwin area. The existence of the cyclone during the convective event is supported by the C-band polarimetric (C-POL) Doppler radar observations and the Tropical eXtended Limited Area Prediction System (TXLAPS) analyses. At 00 UTC on January 24, both C-POL and TXLAPS (not shown) indicate that the center of the cyclone is over the western part of the Tiwi Islands from the surface to 700 hPa, sloping slightly to the NW with height at 500 hPa, and becoming difficult to identify by 300 hPa. The three-hourly C-POL reflectivity at 2.5 km (Figure 4) clearly shows the evolution of cyclonic circulation during the transition of the large MCS from mostly convective (18 UTC) to mostly stratiform (00 UTC).

[18] There are notable differences in cyclone strength and location among different LAM simulations. Of all the simulations shown in Figure 3, WRF-1 appears to predict the central location of the cyclone closest to the observed position, followed by WRF-2 and WRF-3. WRF-4 and MOUM are off-target, while COSMO has a hint of a center near the correct location but elongates the cyclone E-W with two apparent vorticity centers. The different timing and central location of the simulated cyclones may be in part attributed to the specific ways of driving LAMs and different forcing data used in this study (summarized previously in section 2.3) and may be in part due to other differences in model configurations and physics. Also note that the three WRF simulations (WRF-1, WRF-2, and WRF-3) with nudging in the outer domains produced somehow closer location of the low pressure center to the observations than other runs. The different strength of the simulated cyclones apparently depends on the model resolved processes. Some models are able to produce cyclogenesis on a smaller scale while others do not. Note that in WRF-1,

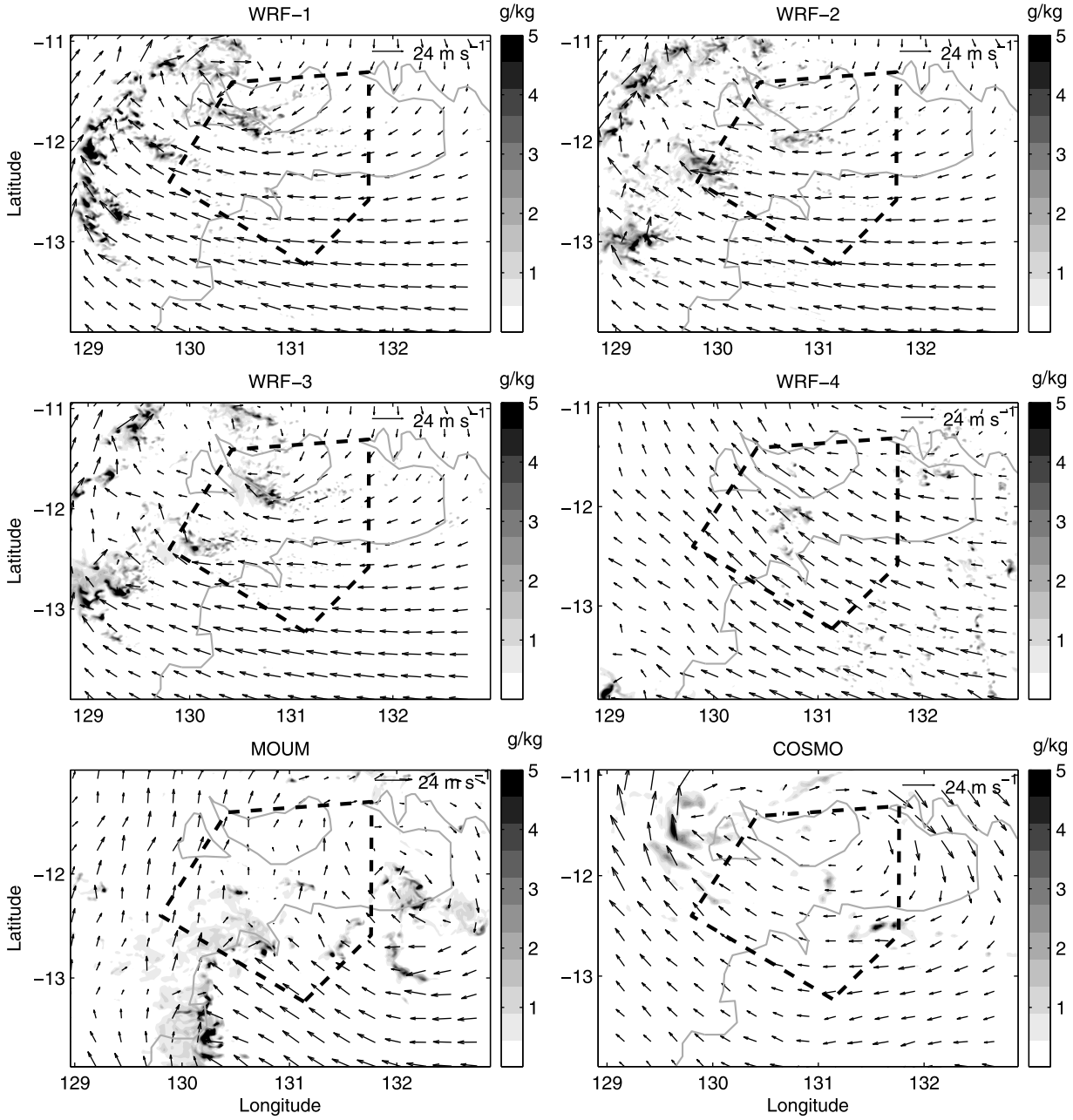

Figure 3. Simulated horizontal wind fields (wind vectors) and hydrometeor mixing ratio (shades) at 2 km height at 01:00 UTC on January 24 from LAMs.

WRF-2, and WRF-3, only changing cloud microphysics results in different cyclone locations. This result shows the importance of the model physics to the cyclone development.

[19] Given the fact that the closed cyclonic flow covers the entire LAM research domain (Figure 3), the conditions at the inflow boundaries should be significantly different from those at the outflow boundaries. This indicates that CRMs, which use periodic lateral boundary conditions, by definition do not support the simulation of cyclonic flow at this scale as the LAMs do. In CRM simulations, the horizontally homogeneous forcings simply filter out all the inhomogeneous features including the cyclone. It is not clear to what extent the simplified forcing and the periodic lateral boundary conditions can affect the explicitly simulated cloud fields. More research on this issue is needed.

[20] A key component of dynamic fields that is critical to convection simulations is the large-scale vertical velocity. In CRMs the large-scale vertical velocity is prescribed as an external forcing. In contrast, the large-scale vertical velocity in LAMs is determined internally during the simulation, which, in this case, is related to the strength of the simulated cyclone. Since the strength of the simulated cyclone depends on both the resolved and parameterized SGS processes, the cross-scale interactions in LAMs could play an important role in determining large-scale horizontal divergence and vertical velocity fields. Figure 5 shows the time-height

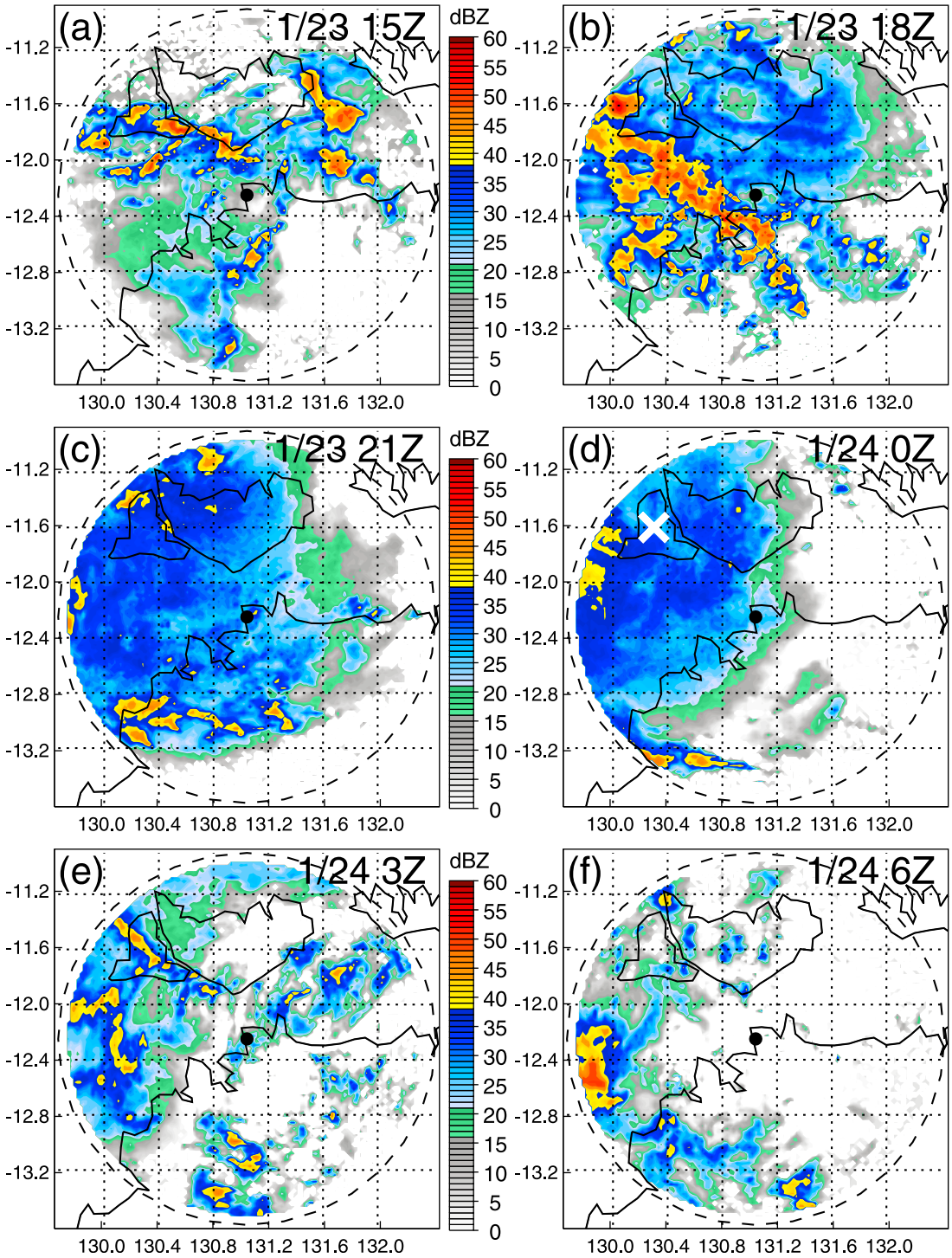

Figure 4. C-POL radar image loop from 15:00 UTC (00:30 LST) January 23 to 06:00 UTC (15:30 LST) January 24. White cross in Figure 4d indicates the location of the surface low pressure center of the cyclone at the time based on the LAPS analysis (higher resolution over smaller area than the TXLAPS analysis).

variation of LAM simulated horizontal divergence averaged over the pentagonal area and the mean vertical profiles averaged over the period from 12 UTC, January 23 to 12 UTC, January 24. All LAMs are able to generate low-level convergence and upper-level divergence during the deep convective event although the time-height pattern simulated by LAMs differs substantially from that of VA. For low-level convergence, the duration in the WRF simulations is too long when compared with the VA. MOUM appears to capture the main characteristics of convergence associated with the observed peak of the deep convective event, but has a large bias elsewhere. COSMO, on the other

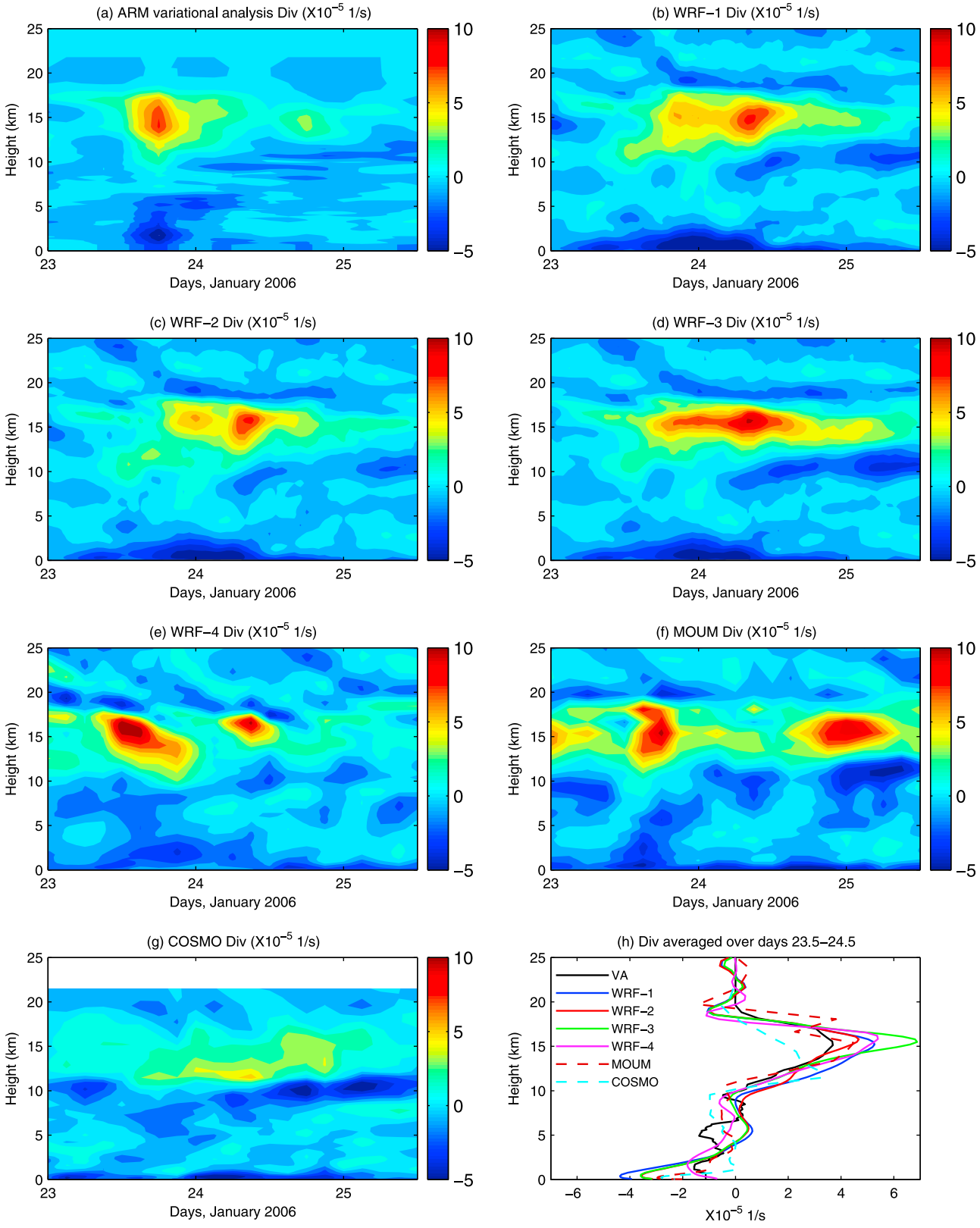

Figure 5. Large-scale horizontal divergence simulated by LAMs averaged over the pentagonal area compared with that of VA. The vertical profiles shown in Figure 5h are averaged over the period from 12:00 UTC January 23 to 12:00 UTC January 24.

hand, does not generate a well-defined low-level convergence structure during the deep convective event. All LAMs except for COSMO over-estimate the upper-level divergence both in magnitude and in duration, while COSMO under-estimates the upper-level divergence during the deep convective event. Despite the apparent difference between the simulations and VA, the vertical structure of LAM simulated mean convergence and divergence over the period that covers the major MCS of Event C matches the VA reasonably well (Figure 5h). In particular, the mean low-level convergence below 10 km simulated by LAMs has a magnitude close to that of VA and has a small inter-LAM spread with the mean standard deviation of 6.2×10^{-6} s^{-1}. It is unknown, however, to what degree the LAM simulations are within the expected experimental uncertainties associated with the VA.

[21] The LAM vertical velocities averaged over the pentagonal area are shown in Figure 6. A promising result is that all LAMs are able to produce the maximum vertical velocity at approximately the same height consistent with the VA. LAMs are inconsistent, however, with the timing and duration of the vertical velocity maximum. Unlike the single peak of vertical velocity during the deep convective event shown in the VA, most of the models show multiple velocity maxima over the period. To better understand this difference, it is helpful to clarify how the large-scale vertical velocities are estimated in the LAM analyses and VA. In the VA, the vertical velocity is mainly estimated from the horizontal divergence/convergence fields, but the radar derived surface precipitation was used as the constraint to conserve the column integrated moisture budget, which has a large impact on the derived large-scale vertical velocity [*Zhang et al.*, 2001]. In contrast, the LAM mean vertical velocity profile is calculated directly by averaging vertical velocity at each grid point, which includes the convective updraft and downdraft associated with clouds. These cloud scale updraft and downdraft are unresolved processes for the VA. Thus, some of the differences shown in Figure 6 may be explained by the different methods of estimating vertical velocity used by the VA and LAM analyses. However, since the vertical velocity basically reflects the deep convective activity, the large inter-LAM spread of vertical velocities and their substantial deviation from the VA indicates that the large-scale dynamic field is not consistently simulated by LAMs. Since large-scale vertical velocity fields in CRMs are prescribed based on the VA, Figure 6 suggests that unlike the large-scale thermodynamic field, the dynamic field in the LAM simulations is substantially different from that in CRMs due to the different forcing strategy and the cross-scale interactions supported by LAMs. This difference in large-scale vertical velocity should have an impact on the cloud fields simulated by LAMs and CRMs.

[22] The temporal evolution of dynamic fields and the interaction with the microphysics may further be inferred from the surface rainfall. Figure 7 shows the surface rainfall from the LAM simulations compared with the estimates from the C-POL radar and the CRM mean. The C-POL rainfall is estimated from the data at 2.5 km elevation and averaged over the circular C-POL domain, which is indicated in Figure 1a and Figure 4 (dashed circle). The CRM mean is averaged over an area equivalent to approximately 176×176 km^2, which is not the whole C-POL area. To make an appropriate comparison with observations, the LAM rainfall rates are averaged over the same area covered by the C-POL radar. The CRM rainfall rates produce a single peak that tracks C-POL rainfall well. This is due to the fact that CRMs are strongly constrained by the large-scale dynamic and thermodynamic forcings. The strong large-scale constraint on CRM rainfall is also reflected by the small inter-CRM spread indicated by the small standard deviation. In the LAMs, the large-scale influence on simulations is only through updating lateral boundary conditions, which is arguably a weaker constraint than that on CRMs, leading to possibly a stronger sensitivity of hydrometeors and precipitation to model physics, the surface inhomogeneity, and the timing and positions of the cyclone in models. It should be noted that the different simulation setup used by LAMs, including the way of initialization, global forcing data, and nudging used or not used in the outer domains, can change the lateral boundary conditions for the innermost research domain of LAMs, leading to different timing and rates of the surface rainfall. As shown in Figure 7, the precipitation peak in some LAMs, particularly, WRF-1, WRF-2, and WRF-3, appears to be delayed by several hours compared with the C-POL estimates. This lag in surface rainfall is consistent with the LAM simulated vertical velocity fields (Figure 6), which mainly reflects that the convective system including the strength, timing, and location of the cyclone associated with the monsoonal trough are not consistently simulated by LAMs.

[23] Compared with observations, COSMO not only fails to capture the right timing of the rainfall peak but also significantly underestimates the magnitude of the peak value. As a result, the mean rainfall rate predicted by COSMO over the period is substantially smaller than the C-POL estimate (inlaid panel in Figure 7). MOUM, on the other hand, is able to simulate the rainfall peak with the right timing and magnitude compared with C-POL. However, it produces a second rainfall peak after the major convective event, which is not supported by observations. Radar and other remote sensing measurements show that the precipitation during the LAM simulation period is mainly dominated by a single major event. The huge explosion of deep convection between 15–18 UTC on January 23 leads to the evolution of a large stratiform rain region and cyclogenesis throughout the low and mid-troposphere. But the observed deep convection, cyclogenesis, and the separated stratiform and convective precipitation are not consistently simulated by LAMs. It also should be pointed out that the estimation of LAM surface rainfall shown in Figure 7 depends on the location of the predicted cyclone. Different LAMs predict different locations for the cyclone. For example, in the COSMO simulations, it is right on the edge of the domain. If all analyses were done centered on the cyclone, perhaps a better agreement on the surface rainfall would be achieved. Thus, compared with the typical CRM analysis methods, the unique LAM simulations also raise a question of how to appropriately analyze the LAM results in a consistent objective way.

[24] Note that compared with other WRF runs, the timing of the rainfall peak predicted by WRF-4 is close to the C-POL estimate. WRF-4 uses a different land surface model, and thus, the timing of rainfall peak may have something to do with land surface processes. To tackle this issue, we

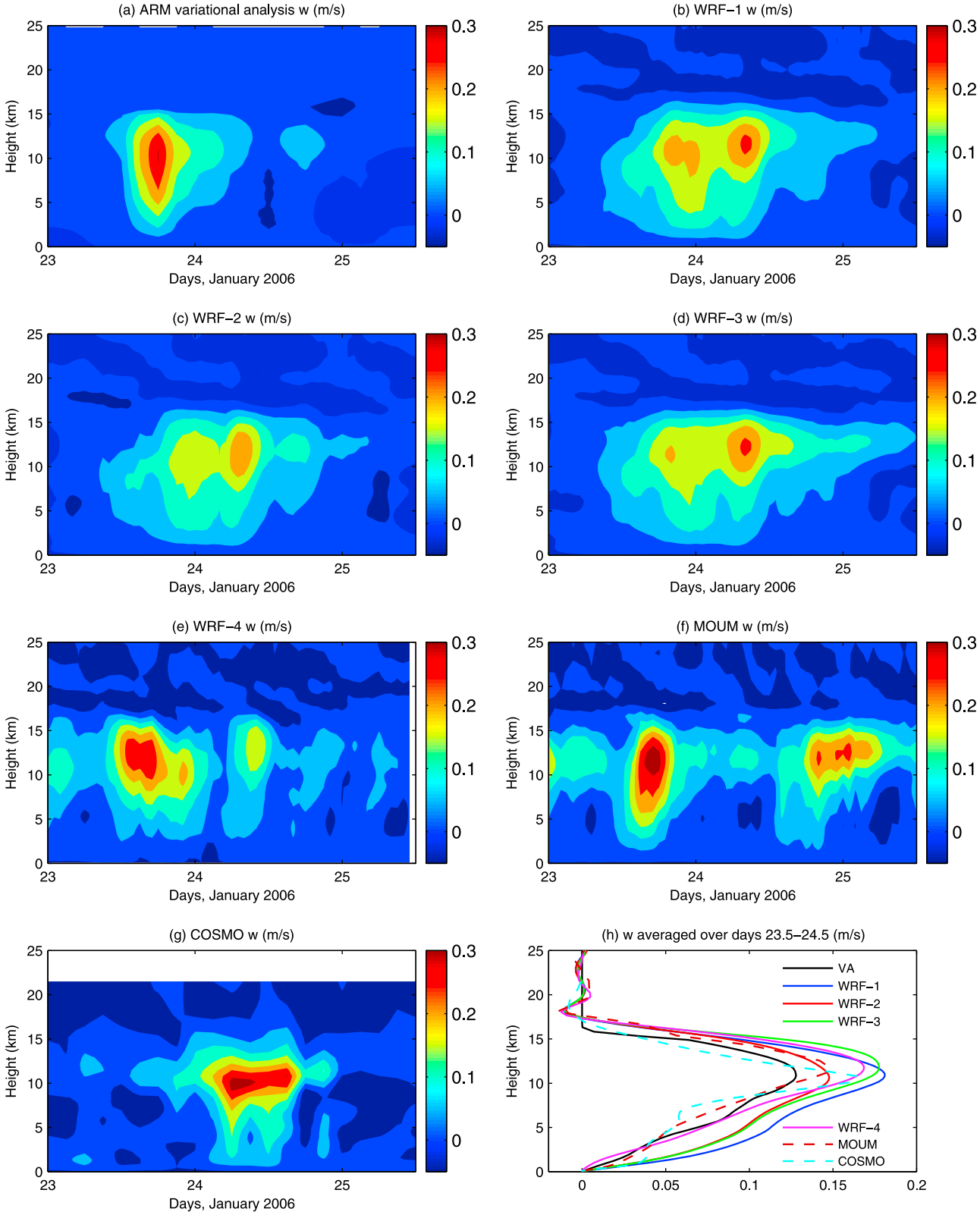

Figure 6. Large-scale vertical velocity simulated by LAMs averaged over the pentagonal area compared with that of VA. The vertical profiles shown in Figure 6h are averaged over the period from 12:00 UTC January 23 to 12:00 UTC January 24.

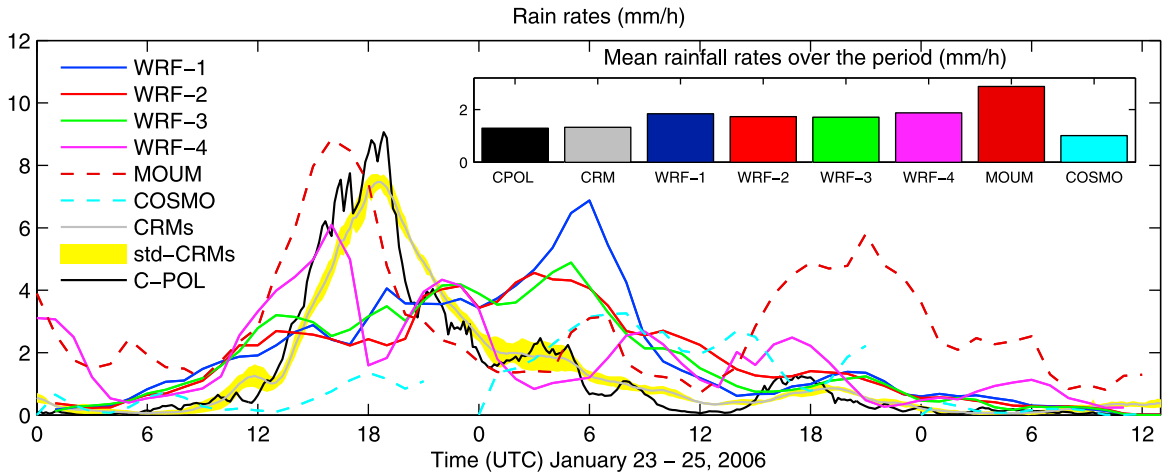

Figure 7. Rain rates from simulations and observations. The rain rate from C-POL radar is at 2.5 km elevation and averaged over the C-POL scanning domain. The LAM results are the surface rain rates averaged over the same area as the C-POL scanning domain. The CRM mean surface rain rate covers the area equivalent to the pentagonal area. The standard deviation of CRM rainfall is indicated by the yellow shades. The inlaid panel shows the mean rainfall rates averaged over the time period.

carefully examined the surface sensible and latent heat fluxes from WRF simulations, but no clear evidence is shown that the land surface processes have an apparent link to the timing of rainfall peak. Note that this difference between WRF-4 and the other WRF runs cannot be explained by whether nudging is on in the outer domains. As shown by Figures 5 and 6, the large-scale dynamics in WRF-4 align more closely with the VA than the other WRF runs with nudging in the outer domains. Thus, we argue that the timing of rainfall (a measure of convection) in LAMs is not controlled by a single process, parameterization, or external forcing; rather, it is determined by a complicated interplay among large-scale forcing through updating lateral boundary conditions, resolved mesoscale processes, and SGS parameterizations that affect large-scale dynamics. This cross-scale interaction poses a challenge for LAMs to realistically simulate tropical deep convective systems.

3.3. Cloud-Scale Dynamic Fields

[25] Cloud-scale vertical velocity plays a key role in determining vertical transport of convective condensate, entrainment processes, and the detrainment of condensate into anvil clouds. Understanding the structure of cloud-scale vertical velocities is also important for the improvement of convection parameterizations. As we showed previously, the large-scale dynamic fields in LAMs are different from those of CRMs. Thus, it is important to examine cloud-scale vertical velocity fields as well. Figure 8 shows the daytime and nighttime in-cloud vertical velocity distributions simulated by LAMs averaged over the pentagonal area compared with the CRM mean. In all simulations, the strong updrafts form a long tail in the histogram. During the daytime (0–6 UTC, or 9:30–15:30 LST), the inter-LAM spread, which is the largest in the convective updrafts, increases with the increasing of height and reaches its maximum near the top of the troposphere. This indicates that without the strong large-scale constraint, the current LAMs have difficulties in generating a consistent cloud-scale vertical velocity field, in particular for convective updrafts. The CRM in-cloud vertical velocity is at the lower end of the distributions. In particular, the convective updrafts are weaker than those of LAMs. The exact reason for weaker CRM vertical velocities is not clear but may be due to the fact that the dynamic field in CRMs is strongly constrained by the prescribed large-scale vertical velocity profile. The differences exhibited by the in-cloud vertical velocity distributions between LAMs and CRMs may also be caused by the differences in the location of the cyclone as well as the land-initiated convection in LAMs that is not simulated by CRMs. The convective updrafts during the night (12:00–18:00 UTC or 21:30–3:30 LST) are much stronger than those during the day. This is consistent with the fact that the strongest deep convection occurs in the evening of 23 January. Note that due to the logarithmic scale used in Figure 8, it is impossible to add the inter-CRM spread (standard deviation) in the figure. The results show that similar to that of LAMs, the larger inter-CRM spread is in the convective updrafts.

[26] To further characterize the cloud-scale vertical velocity fields simulated by LAMs, we examined the mean in-cloud vertical velocity over the pentagonal area during the period when the major MCS occurred. Figure 9 shows the mean profiles along with the CRM results. Unlike the domain mean profile that has a sole vertical velocity maximum in the upper troposphere, WRF-1, WRF-2, and WRF-3 show a second peak circa 4 km. This double-peak structure, however, is not clearly seen in WRF-4, MOUM, COSMO, and CRMs. Although the upper level peak of in-cloud vertical velocity occurs approximately at the same height as that of the domain-mean vertical velocity profiles (Figure 6h), the peak magnitude between models varies. The peak in WRF-1, WRF-2, WRF-3, and MOUM is nearly twice as large as that in WRF-4, COSMO, and CRMs. Leaving aside the detailed differences between models, the most important conclusions to draw here are: First, the mean in-cloud vertical velocity profiles do not share the same vertical structure as the domain mean vertical velocity profiles. Second, the fact that the inter-LAM spread shown in Figure 9 is larger than that seen in Figure 6h suggests that the mean in-cloud

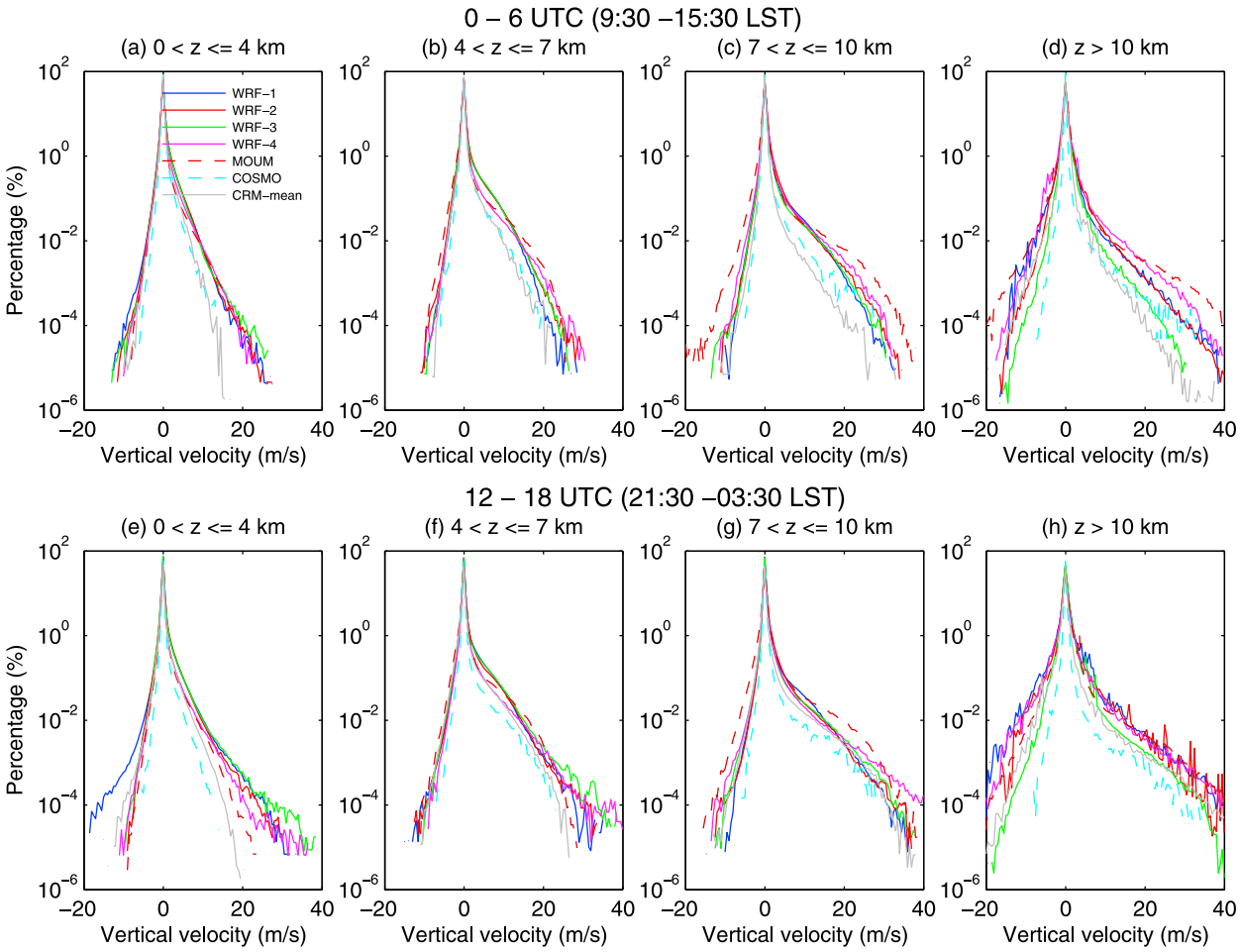

Figure 8. LAM simulated in-cloud vertical velocity PDF over the pentagonal area for two periods: 00:00–06:00 UTC (9:30–15:30 LST) and 12:00–18:00 UTC (21:30–3:30 LST) January 23, 2006. The CRM results are the mean from seven baseline runs.

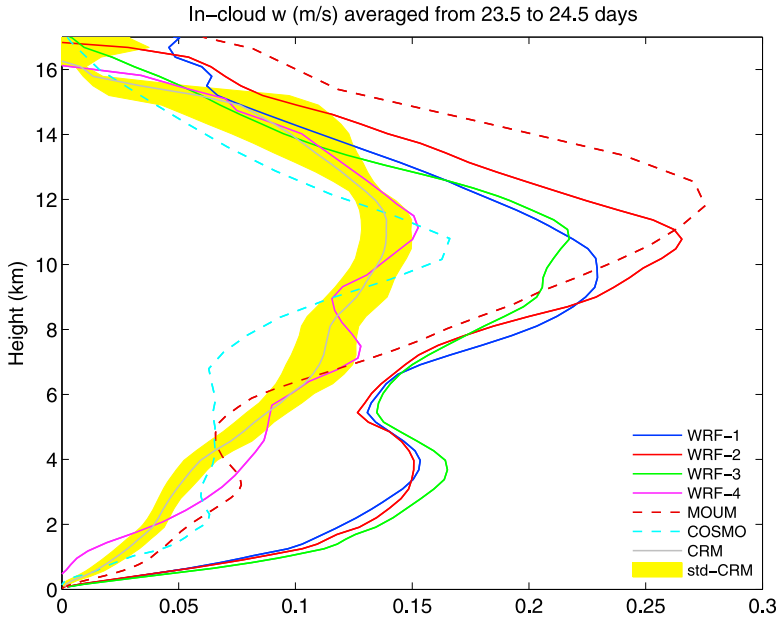

Figure 9. LAM simulated in-cloud vertical velocity profiles over the pentagonal area averaged over the period from 12 UTC January 23 to 12 UTC January 24 compared with the CRM results.

vertical velocity is more sensitive to specific model configurations and physics than the domain mean vertical velocity. The large uncertainty in cloud-scale dynamics is a challenge for LAMs and needs to be further investigated in future studies.

3.4. Cloud Fields

[27] One focus of this study is to evaluate whether cloud properties associated with the monsoonal deep convective systems can be realistically simulated by LAMs and examine the sensitivity of explicitly simulated clouds to model configurations and microphysics. In this study, clouds in LAMs and CRMs are defined wherever the grid box total mixing ratio of cloud water, rain, ice, snow, and graupel exceeds 10^{-6} kgkg^{-1}. For MOUM, although there is also an actual subgrid cloud scheme to determine the grid-box cloud cover, it is not used in the analyses. Figure 10 shows the time-height variation of cloud fraction averaged over the pentagonal area from LAMs compared with the cloud fraction in the VA data set, which is derived from the Active Remotely Sensed Cloud Locations (ARSCL) [*Clothiaux et al.*, 2000; *Xie et al.*, 2010b] retrievals, and the mean cloud fraction from the seven baseline CRMs. As a further comparison, the time variation of vertically integrated high clouds from LAMs, CRMs, and those derived from the Multifunctional Transport Satellite (MTSAT) retrievals are also shown in the figure. Here, following the International Satellite Cloud Climatology Project (ISCCP), high clouds are defined above 440 hPa. Note that the ARSCL retrievals are derived from the vertical pointing cloud radars, thus, the comparison between the temporal ARSCL cloud fraction and the spatial cloud fraction from models should not be interpreted as an exact comparison. Also note that the satellite measured low cloud fractions are nearly zero, which is caused by the obscuration from mid and high clouds (overcast in this case) due to the 'top-down' satellite view, and thus, no low cloud comparison is shown here. As shown by the figure, there is a large disparity between LAMs, CRMs, and observations. WRF-1, WRF-2, and WRF-3 fail to produce large cloud fractions during the convective event compared with the ARSCL retrievals and CRMs. This error appears to be consistent with the surface rainfall delay in these simulations shown in Figure 7. WRF-4, on the other hand, predicts a large amount of clouds during the deep convective event. Compared with the WRF simulations, MOUM and COSMO show different time-height structure of cloud fraction. MOUM appears to capture some of the vertical cloud fraction structure during the main precipitation event but has large errors elsewhere compared with the ARSCL retrieval. COSMO predicts excessive cloud fractions throughout the simulation period, especially in the upper troposphere.

[28] A diurnal variation of high clouds is seen in the WRF simulations. Although the phase of diurnal variation seems to be consistent with the satellite observations, the simulated amplitude of diurnal variation is much larger than observed. The high clouds simulated by MOUM also show a somewhat diurnal variation, but its phase is off compared to observations. However, we note that MOUM agrees better with the CRMs, particularly for the times toward the end of the simulation period. The high clouds simulated by COSMO do not show diurnal variation, but nearly 100% cloud cover is consistent with satellite observations. CRMs also produce a large amount of high clouds due to the long lifetime of cirrus and the periodic boundary conditions which keep them in the domain, but no clean diurnal variation is seen in the CRM simulations. The different diurnal variations of high cloud fraction simulated by LAMs and CRMs indicate that the processes that govern the high cirrus clouds associated with the monsoonal deep convective system are not consistently modeled in cloud resolving simulations.

[29] To further illustrate the differences and similarities of simulated clouds, Figure 11 shows the vertical profiles of individual types of hydrometeor mixing ratios over the pentagonal area averaged over the period from 12 UTC January 23 to 12 UTC January 24. Since the MOUM microphysics scheme uses a single prognostic moment to Represent the solid phase hydrometeor, no individual mixing ratios for ice, snow, and graupel are provided. Also note that the non-zero rainwater mixing ratio above the homogeneous freezing level in the MOUM run is caused by a bug. This bug has been fixed in the latest model version. In WRF and COSMO, the thresholds of size and fall speed to define ice and snow depend on specific cloud microphysical schemes. Generally, ice has a negligible fall speed and a mean diameter smaller than snow. Large inter-model spreads are shown for all types of hydrometeors. In some types, ice, snow, and graupel, for example, the large inter-LAM differences can be up to a factor of 10. The cause of the huge inter-LAM spread is complex. Different forcing data, lateral boundary conditions for the innermost domain, model physics and configuration including resolution can all lead to the difference in simulated cloud hydrometeors. Even the definition of ice, snow, and graupel may be different depending on the specific microphysical schemes used in the simulations, which may explain part of the inter-model spread. The inconsistency in simulated cloud hydrometeors is also shown by the large standard deviation of CRMs. Considering that the differences due to the large-scale forcing have been minimized in the CRM simulations, the large standard deviation indicates the great sensitivity of simulated cloud hydrometeors to model physics and configuration.

[30] Since WRF-1, WRF-2, and WRF-3 are exactly the same except for the cloud microphysics scheme used, the difference between them should provide a measure of the sensitivity of the simulated hydrometeor content to microphysics in the LAM framework. One of the major differences among them is the distribution of solid phase hydrometeors between ice, snow, and graupel. The Thompson scheme (WRF-1) produces a large amount of snow but little ice and graupel compared with the other WRF runs. This result may be explained by the smaller fall speeds of snow in the Thompson scheme. Figure 7 shows that WRF-1 has similar rainfall to WRF-2 and WRF-3, and thus, to achieve that with far less graupel than WRF-2 and WRF-3 requires a large amount of snow. On the other hand, the WSM-6 and Morrison schemes agree on graupel contents, but disagree on cloud ice and snow content. This difference may be due to the different snow-ice threshold used in the scheme. In total, the Thompson scheme produces more solid phase hydrometeor content than the WSM-6 and Morrison schemes. It is important to point out that the differences shown in WRF-1, WRF-2, and WRF-3 include both the

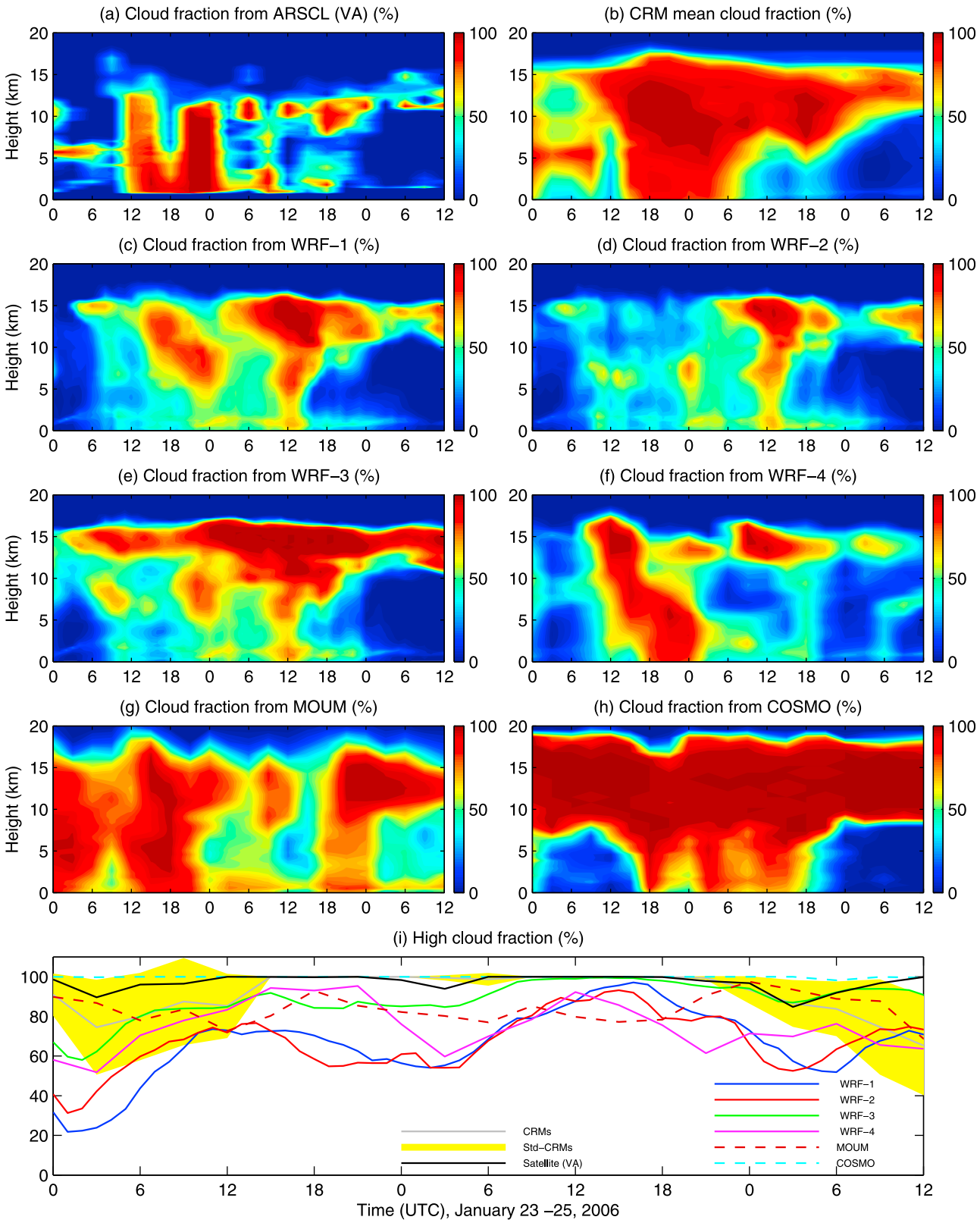

Figure 10. LAM simulated cloud fraction averaged over the pentagonal area compared with the CRM mean and the ARSCL retrievals from VA. Figure 10i shows high cloud fraction from LAMs, CRMs, and satellite retrievals, respectively.

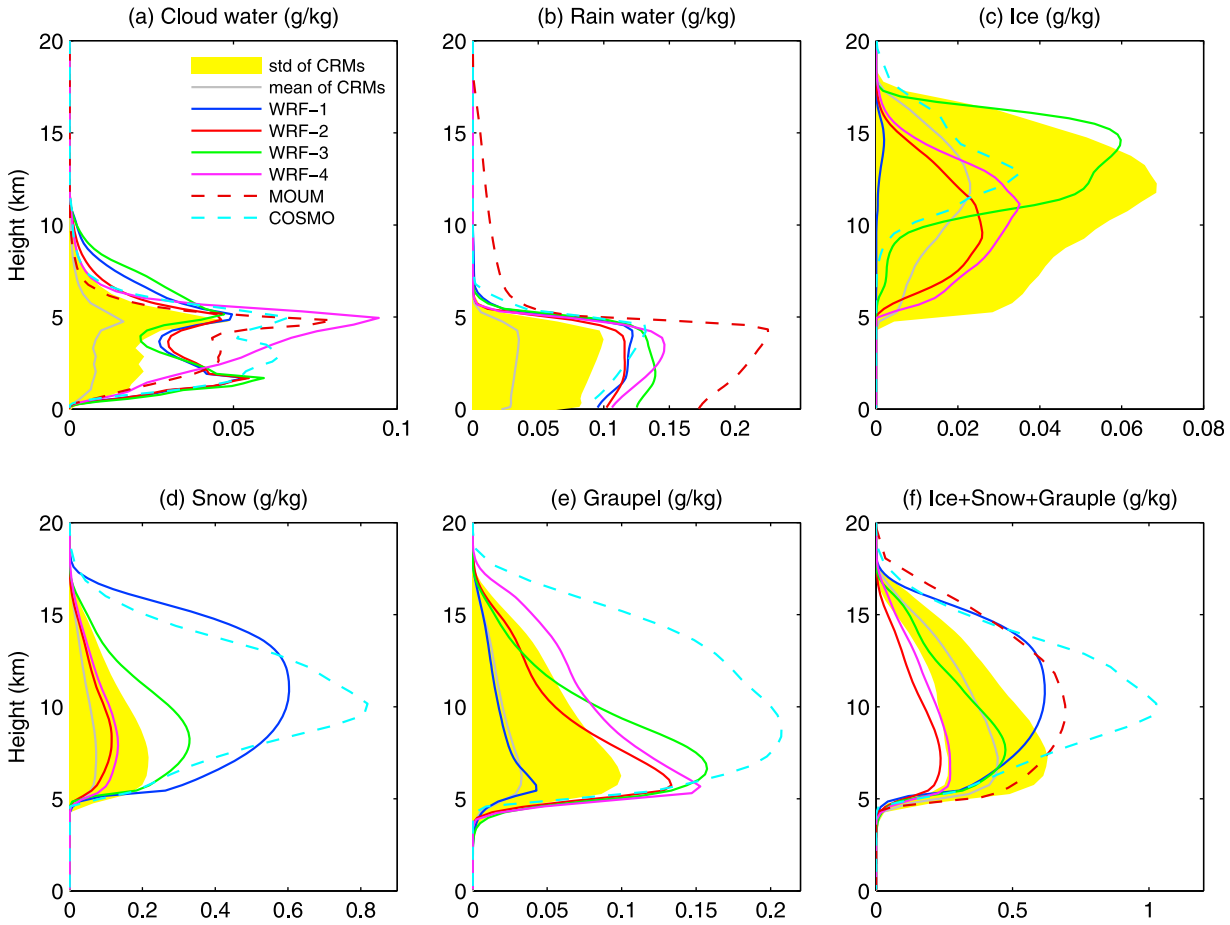

Figure 11. Vertical profiles of (a) cloud water, (b) rain water, (c) ice, (d) snow, (e) graupel, and (f) sum of solid phase hydrometeor mixing ratios over the pentagonal area averaged over the period from 12 UTC January 23 to 12 UTC January 24. The CRM results are from seven baseline runs over the same period. The standard deviations of CRM results are indicated by the yellow shades.

direct sensitivity of hydrometeor content to microphysics (a sensitivity that can be measured by CRMs) and the indirect sensitivity due to the differences in the lateral boundary conditions for the innermost domain caused by the cross-scale interaction in the two-way nested LAMs. Note that this cross-scale interaction has been suppressed in the WRF-1, WRF-2, and WRF-3 simulations due to the nudging used in the outer domains. This indirect impact adds difficulties in evaluating the sensitivity of simulated cloud fields to microphysics in the LAM framework.

[31] Since cloud radiative properties (e.g., cloud fraction and hydrometeor content) and precipitation are intimately linked to cloud scale dynamics, particularly the in-cloud vertical velocities, it is useful to examine the cloud properties in different dynamic regimes. To do so, we carried out statistical analyses of the LAM simulated clouds using conditional sampling based on the in-cloud vertical velocity, and classified them into three categories as follows: convective clouds if the absolute value of vertical velocity in a cloudy grid cell is greater than 3 m s^{-1}; stratiform clouds if the absolute value of vertical velocity in a cloudy grid cell is smaller than 1 m s^{-1}; and transitional clouds if the absolute value of vertical velocity in a cloudy grid cell is between 1 m s^{-1} and 3 m s^{-1}.

[32] Figure 12 shows the conditionally sampled fraction of liquid and solid phase hydrometeors over the pentagonal area averaged over the period from 12 UTC January 23 to 12 UTC January 24 from the LAM and CRM simulations. Despite the large inter-model spread, all models agree that the largest cloud fraction is associated with the stratiform solid phase hydrometeors (Figure 12d) and convective hydrometeors (Figure 12f) occupy less than 3 percent of the total cloudy area. For comparison, the area coverage fractions defined solely based on vertical velocities are also shown in Figures 12g, 12h, and 12i. It appears that the fractions of transitional and convective solid phase hydrometeors (Figures 12e, 12f) are very close to the fractions of transitional and convective vertical velocities (Figures 12h and 12i). Note that the similarity is not only in the magnitude of fraction but also in the vertical structure of fraction profiles, suggesting that the areas with $|w| \geq 1$ m s^{-1} are covered by clouds. In contrast, the vertical structure of stratiform solid hydrometeor fraction (Figure 12d) is completely different from that of stratiform vertical velocities (Figure 12g) although in some cases (e.g., COSMO) the value of maximum fraction of stratiform solid hydrometeors is close to the fraction of vertical velocity. Previously, Figure 10 showed that COSMO produced excessive cloud

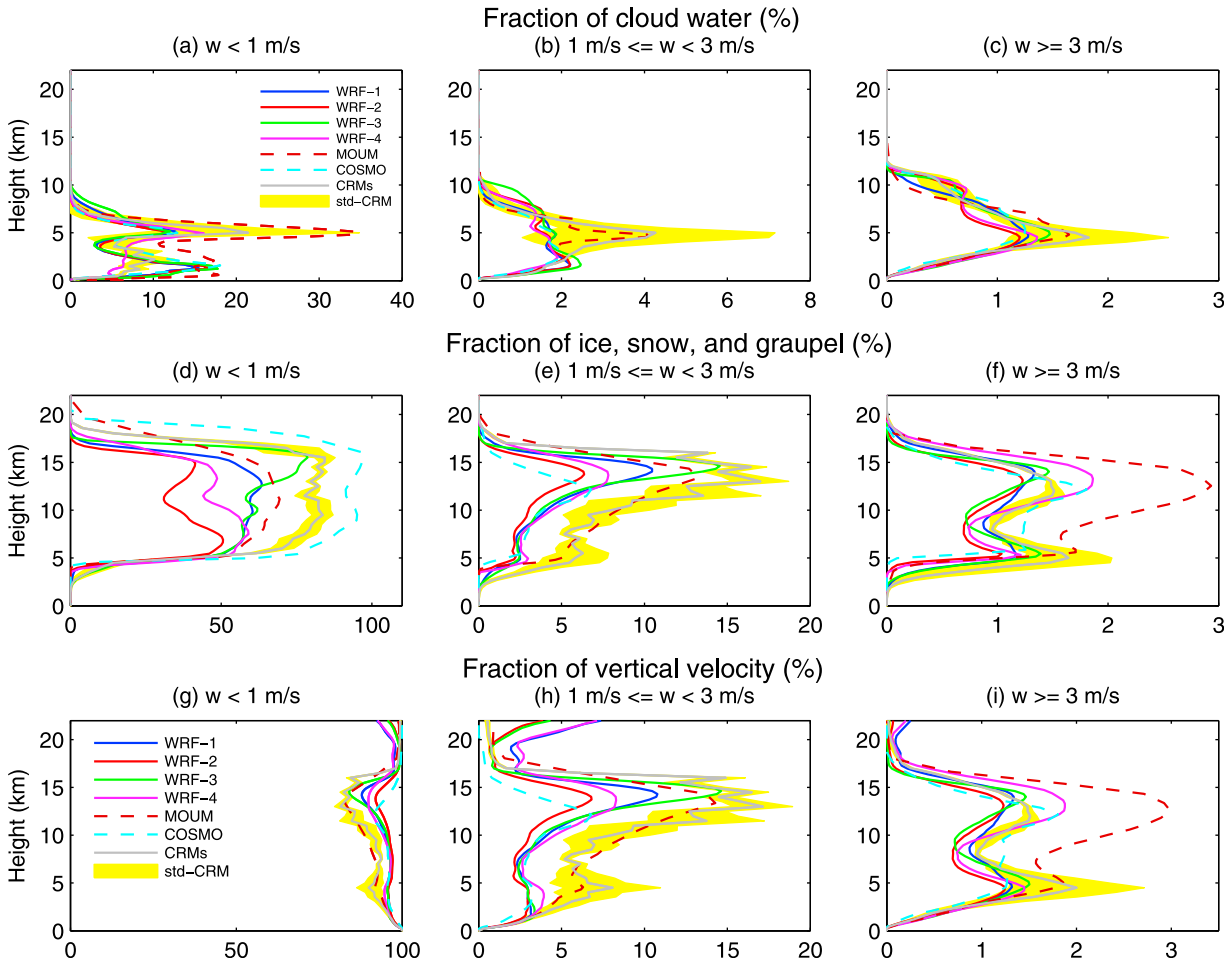

Figure 12. (a–f) Fractions of liquid and solid phase cloud hydrometeors conditionally sampled based on vertical velocity: $|w| < 1$ m s^{-1} (stratiform); 1 m s^{-1} $\leq |w| < 3$ m s^{-1} (transitional); and $|w| \geq 3$ m s^{-1} (convective) over the pentagonal area averaged over the period from 12 UTC January 23 to 12 UTC January 24. (g–i) Total area coverage in percentage (cloudy and clear) for three vertical velocity range: $|w| <$ 1 m s^{-1}; 1 m s^{-1} $\leq |w| < 3$ m s^{-1}; and $|w| \geq 3$ m s^{-1}.

fractions close to 100 percent. Figure 12d further reveals that the large cloud fraction is caused by the stratiform solid phase clouds.

[33] Figure 12 also shows that the CRM mean generally falls in the range of LAMs except for the transitional regime (Figures 12b, 12e, and 12h) where the CRM results are at the high end of LAMs, close to the MOUM results. This is a promising result considering the two totally different numerical approaches, and once again suggests a certain consistency (or may be considered as a degree of success) of LAM and CRM simulations of this case.

[34] Using the LAM and CRM output we also examined the LAM and CRM simulations outside the deep convection period. The analyses show some interesting similarities and differences among LAM and CRM simulations. As an example, Figure 13 shows the fraction of transitional and convective solid phase hydrometeors averaged over the period from 12 UTC January 24 to 12 UTC January 25 when the major MCS associated with Event C has left the research domain. As shown in the figure, MOUM and WRF-3 produced much larger cloud fractions than other models. The large fraction of transitional and convective solid phase clouds generated by MOUM is possibly related to the underrepresentation of vertical mixing in the upper troposphere. In MOUM, there is no vertical mixing parameterization above the diagnosed boundary layer. While the cause for MOUM generating a large fraction of transitional and convective solid phase clouds may be complicated, the large deviation in WRF-3 from WRF-1 and WRF-2 can be solely attributed to the cloud microphysics. The reason for the Morrison scheme producing a larger amount of transitional and convective solid phase clouds than other schemes after the major MCS is unclear, but it suggests that future evaluation and improvement of the Morrison scheme should focus on high clouds associated with relatively large vertical velocities.

[35] Figure 14 shows the conditionally sampled hydrometeor mixing ratios based on vertical velocity over the pentagonal area averaged over the period from 12 UTC January 23 to 12 UTC January 24. Despite the fact that the stratiform solid phase clouds dominate the cloud fraction (Figure 12d), they only contain a very small hydrometeor content, about one tenth of convective plus transitional solid phase clouds. This ratio appears to be robust since it is supported by all LAM and CRM simulations. However,

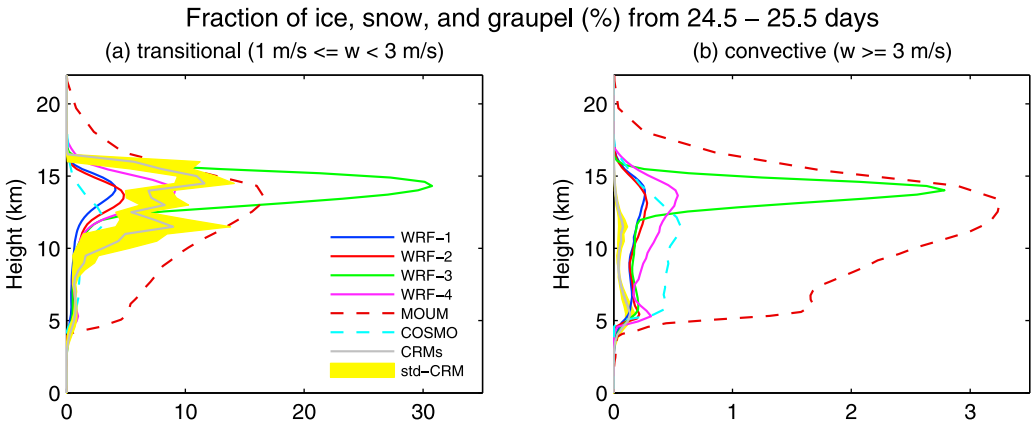

Figure 13. Fractions of (a) transitional and (b) convective solid phase cloud hydrometeors over the pentagonal area but averaged over the period from 12 UTC January 24 to 12 UTC January 25.

there is a large inter-LAM spread in all categories of hydrometeor mixing ratio, suggesting that to obtain a consistent hydrometeor content associated with tropical convective systems is a big challenge for cloud resolving simulations. One of the primary causes for the uncertainty is the different cloud microphysics schemes. This is supported by the results of WRF-1, WRF-2, and WRF-3, which only differ in microphysics. The conditionally sampled CRM hydrometeor mixing ratios are generally within the range of LAM statistics. However, in some categories, such as the

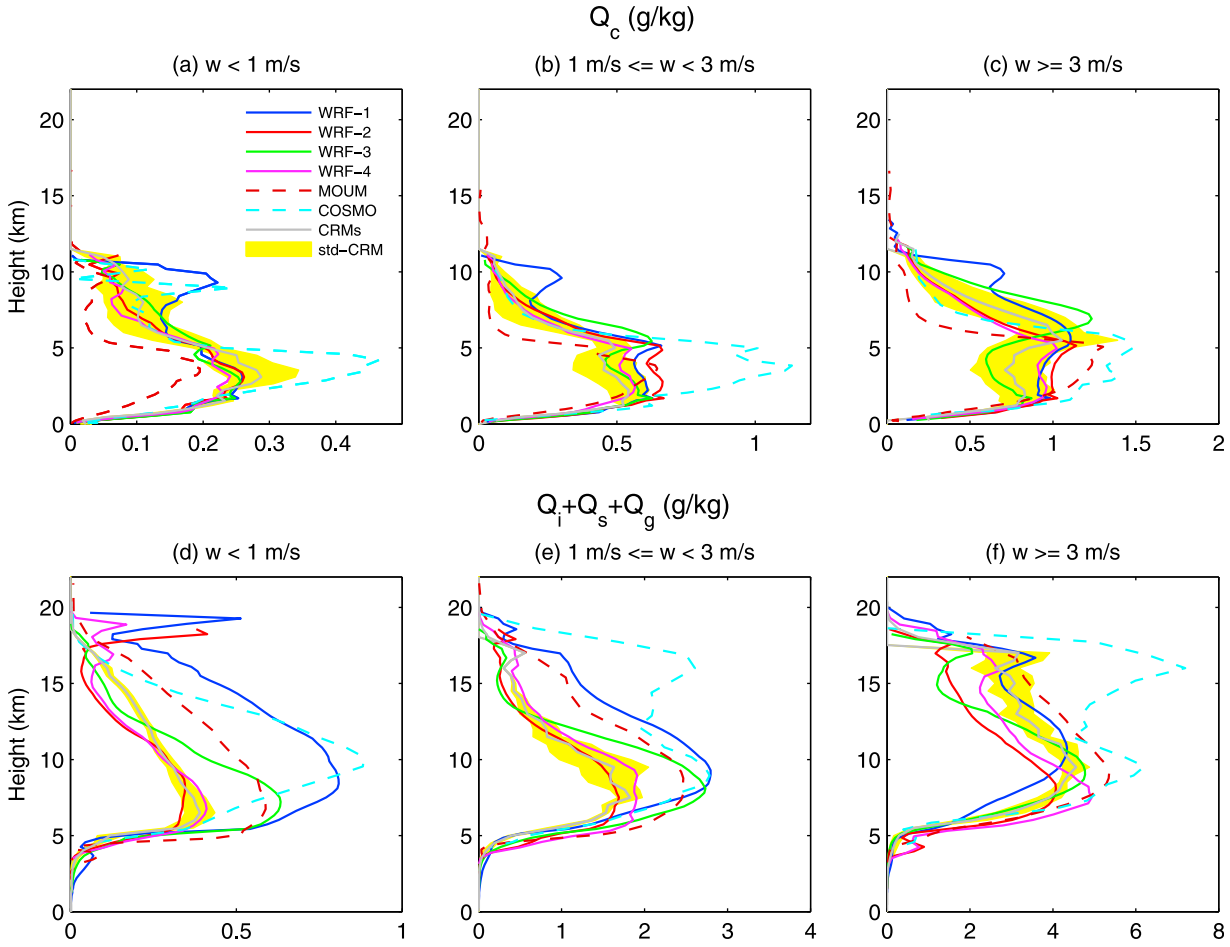

Figure 14. Liquid and solid phase hydrometeor mixing ratios conditionally sampled based on vertical velocity: $|w| < 1$ m s^{-1} (stratiform); 1 m s^{-1} $\leq |w| <$ 3 m s^{-1} (transitional); $|w| \geq 3$ m s^{-1} (convective). The profiles are averaged over the pentagonal area and from 12 UTC January 23 to 12 UTC January 24.

transitional solid hydrometeor content (Figure 14e), the CRM results are at the lower end of the LAM results. This is in contrast to the fraction of transitional solid phase clouds (Figure 12e) where the CRM mean is at the high end of the LAM results. It is not clear why CRMs consistently (indicated by the small standard deviations) predict larger cloud fraction and smaller hydrometeor content for transitional ice clouds relative to LAMs. Further investigation is needed.

4. Summary and Discussion

[36] In this ARM/GCSS/SPARC numerical simulation intercomparison study, cloud-resolving LAMs are configured to simulate the strongest deep convective event observed during the TWP-ICE field experiment. A total of six LAM simulations with different configurations from three models, namely, WRF, MOUM, and COSMO, participated in this study. LAM simulations are compared against observations, primarily the ARM VA product [*Xie et al.*, 2010a] that integrates all available ARM observations in a consistent and objective way, and the CRM simulations submitted to the accompanying TWP-ICE CRM intercomparison study [*Fridlind et al.*, 2010]. Using these intercomparisons, we have assessed (1) how well the dynamic and thermodynamic fields of a TWP-ICE active monsoonal mesoscale convective event can be reproduced by LAMs and (2) whether the LAM results can be statistically compared to those of CRMs if both LAMs and CRMs are configured at the equivalent resolution. The results are summarized as follows:

[37] 1. Driven by the ECMWF analyses or global model forecasts, all LAMs are able to reproduce realistic mean potential temperature profiles during the active monsoon phase consistent with the VA. Although there is a relatively large inter-LAM spread in relative humidity profiles in the upper troposphere, the spread is modest below 10 km with a mean standard deviation of 2.7% and is fairly consistent with the VA and CRM mean, suggesting that the global forcing data does provide a first order approximation of large-scale thermodynamic fields for LAMs. It also suggests that the ECMWF analyses or GME forecasts can provide sufficiently accurate thermodynamic fields compared to those of VA, which make it possible to compare the LAM simulations with the CRM simulations forced by the VA, at least from the large-scale thermodynamic forcing perspective.

[38] Compared with the reasonably well simulated large-scale thermodynamic fields, the LAM simulated large-scale horizontal divergence and vertical velocity fields show a large inter-model spread and deviate substantially from those of VA. The cause for the inconsistent simulations of the deep convective event by LAMs is complex. Different model dynamic core, physics, resolution, the way of nesting and initialization, nudging in the outer domains, and large-scale forcing data can all lead to different cross-scale interactions in LAMs, which are mainly responsible for the different strength, location, and timing of the simulated explosive deep convection and the subsequent cyclogenesis. Thus, although the unique capability to support cross-scale interactions of LAMs has a clear advantage over the horizontally homogeneously forced CRMs, how to obtain consistent and reliable dynamic fields under a weak large-scale constraint is a challenge for LAMs. Since the vertical velocity is prescribed in CRMs based on the VA, the large deviation of LAM simulated vertical velocity fields from the VA indicates that there is an important difference in dynamic forcing in the CRM and LAM simulations for this TWP-ICE case.

[39] 2. Despite the differences in large-scale forcing, the CRM and LAM simulations do show certain consistency in the simulated cloud fields. For example, both CRMs and LAMs agree that the largest cloud fraction is associated with the stratiform ($w \leq 1$ m s^{-1}) solid phase clouds and convective (w > 3 m s^{-1}) clouds occupy a very small part (less than 3 percent in this case) of the total cloudy area. However, although the stratiform solid phase clouds dominate the cloud fraction, they only contain a very small hydrometeor content, about one tenth of convective plus transitional (1 m s^{-1} < $w \leq 3$ m s^{-1}) solid phase clouds. Moreover, except for a few exceptions where the CRM mean is either at the low end or at the high end of the LAM results, the mean of CRM simulated cloud properties generally falls in the range of LAMs. Considering the two totally different numerical approaches, this consistency between the CRM and LAM simulations can be considered as some degree of success in cloud resolving simulations of this TWP-ICE case.

[40] However, the detailed intercomparison shows that the difference between CRM and LAM simulations and the inter-LAM differences are significant enough to be addressed. LAMs disagree markedly on their predicted cloud fraction and hydrometeor mixing ratio, particularly for solid phase hydrometeors: cloud ice, snow, and graupel. The inter-LAM difference of some specific types of hydrometeors can be a factor of 10. Conditionally sampled clouds based on the vertical velocity clearly reveal that the stratiform solid phase clouds associated with the major MCS are the least consistent cloud types in the LAM simulations. The large inter-LAM spread suggests high sensitivity of the simulated clouds to changes in large-scale dynamics (e.g., the strength and location of the cyclone), thermodynamic fields, and model physics and configuration, but may also reflect the fact that the cloud-scale processes in LAMs are loosely constrained (via updating the lateral boundary conditions), which introduces additional variability in the LAM simulations.

[41] This study demonstrates that the LAM approach possesses a unique capability in simulating tropical deep convection and has the potential to bridge the gap between NWPs and CRMs. In addition to the findings summarized previously, this first ever LAM/CRM intercomparison on the TWP-ICE deep convective case also raises some questions that need to be further investigated in future studies. As we showed in this study, due to their specific forcing strategy, CRMs are incapable of simulating some important dynamic features, such as the meso-cyclogenesis in this case. While LAMs possess the ability to capture these dynamic features, it is at the cost of losing strong large-scale dynamic constraint. Although the intercomparison clearly reveals important differences in the simulated clouds by the two methods, we are unable to quantify the effect of different dynamic forcing on clouds since it is intertwined with other effects. Two questions need to be addressed in future CRM and LAM studies. For CRMs, since they assume horizontally homogeneous and use prescribed vertical profiles and large-scale forcing, it is not clear to what extent the oversimplified large-scale fields and forcing can affect the fidelity of the

simulated cloud fields. For cloud-resolving LAMs, the problem arises from their forcing strategy. The lateral boundary conditions for the innermost domain are not prescribed but are determined through nesting, which introduces an extra uncertainty in the LAMs simulations. It is not clear how large this uncertainty is compared with other uncertainties caused by other processes and how this uncertainty affects the explicitly resolved cloud fields. These questions are important and need to be addressed since the CRM approach has been used in super parameterization to represent deep convection and associated clouds in GCMs and the nesting technique used by LAMs has the potential to be used in future climate simulations. To answer these questions, more CRM/LAM intercomparisons on different cases, both dynamically active cases like this one and less dynamically active cases, should be carried out. In this study, we have shown that conditional sampling is a useful tool to identify similarities and differences in clouds. Such a method could be extended and applied in future studies on cases in which large-scale conditions are not well captured by LAM simulations. In this study, LAMs use different large-scale forcing data and different ways (including nudging) to generate lateral boundary conditions for the innermost research domain. This adds difficulties in identifying the causes for the inter-LAM differences. In future LAM intercomparison studies, to reduce the uncertainty in large-scale forcing, the same large-scale forcing data and nudging with the same strength in the outer domains are recommended to generate more consistent lateral boundary conditions for the LAM research domain. Moreover, to obtain a stronger large-scale dynamic constraint, one could nudge high resolution analysis or observations directly into the LAM research domain at different nudging strengths and timescales. These practices should be tested and examined in future LAM studies.

[42] **Acknowledgments.** Ping Zhu wishes to acknowledge his support for this work by the DOE ASR program under grant DE-FG02-09ER64737 and National Science Foundation (NSF) under grant ATM-0735954. Jim Dudhia acknowledges his support by DOE ASR grant DE-FG02-08ER64575 and NSF support for computational resource for his simulation. Ann Fridlind acknowledges her support from DOE ARM program grants DE-AI02-06ER64173, DE-AI02-08ER64547, and DE-FG03-02ER63337. Support for A. Varble and E. Zipser is acknowledged from DOE ARM grant DEFG0208ER64557. The CRM computational support was provided by the DOE National Energy Scientific Computing Center and the NASA Advanced Supercomputing Division. We thank the TWP-ICE field campaign team led by Peter May. TWP-ICE data were obtained from the ARM program archive, sponsored by the DOE Office of Science, Office of Biological and Environmental Research, Environmental Science Division. We thank ECMWF for kindly providing their analyses data to support the TWP-ICE modeling studies. We are very grateful to the three anonymous reviewers for their constructive comments. Their helpful suggestions led to substantial improvement of this paper.

References

Arakawa, A. (2004), The cumulus parameterization problem: Past, present, and future, *J. Clim.*, *17*, 2493–2525.

Chen, F., and J. Dudhia (2001), Coupling an advanced land surface hydrology model with the Penn State/NCAR MM5 modeling system. Part 1: Model description and implementation, *Mon. Weather Rev.*, *129*, 569–586.

Clothiaux, E. E., T. P. Ackeman, G. G. Mace, K. P. Moran, R. T. Marchand, M. A. Miller, and B. E. Martner (2000), Objective determination of cloud height and radar reflectivities using a combination of active remote sensors at the ARM CART sites, *J. Appl. Meteorol.*, *39*, 645–665.

Cullen, M. J. P., T. Davies, M. H. Mawson, J. A. James, S. C. Coulter, and A. Malcolm (1997), An overview of numerical methods for the next generation UK NWP and climate model, in *Numerical Methods in Atmospheric and Ocean Modelling: The Andre J. Robert Memorial Volume*, edited by C. A. Lin, R. Laprise, and H. Ritchie, pp. 425–444, Can. Meteorol. and Oceanogr. Soc., Ottawa, Ont., Canada.

Davies T., M. J. P. Cullen, A. J. Malcolm, M. H. Mawson, A. Staniforth, A. A. White, and N. Wood (2005), A new dynamical core for the Met Office's global and regional modelling of the atmosphere, *Q. J. R. Meteorol. Soc.*, *131*, 1759–1782.

Del Genio, A. D., and W. Kovari (2002), Climatic properties of tropical precipitating convection under varying environmental conditions, *J. Clim.*, *15*, 2597–2615.

Del Genio, A. D., and M. S. Yao (1988), Sensitivity of a global climate model to the specification of convective updraft and downdraft mass fluxes, *J. Atmos. Sci.*, *45*, 293–318.

Drosdowsky, W. (1996), Variability of the Australian summer monsoon at Darwin: 1957–1992, *J. Clim.*, *9*, 85–96.

Dudhia, J. (1989), Numerical study of convection observed during the winter monsoon experiment using a mesoscale two-dimensional model, *J. Atmos. Sci.*, *46*, 3077–3107.

Essery, R. L. H., M. J. Best, R. A. Betts, P. M. Cox, and C. M. Taylor (2003), Explicit representation of subgrid heterogeneity in a GCM land surface scheme, *J. Hydrometeorol.*, *4*, 530–543.

Fridlind, A., A. Ackerman, J. Petch, P. Field, A. Hill, G. McFarquhar, S. Xie, and M. Zhang (2010), ARM/GCSS/SPARC TWP-ICE CRM Intercomparison Study, *NASA Tech. Memo.*, *NASA-TM-2010-215858*, 30 pp.

Fridlind, A. M., et al. (2012), A comparison of TWP-ICE observational data with cloud-resolving model results, *J. Geophys. Res.*, *117*, D05204, doi:10.1029/2011JD016595.

Gregory, D., and P. R. Rowntree (1990), A mass flux convection scheme with representation of cloud ensemble characteristics and stability-dependent closure, *Mon. Weather Rev.*, *118*, 1483–1506.

Heise, E., and R. Schrodin (2002), Aspects of snow and soil modeling in the operational short range weather prediction models of the German Weather Service, *J. Comput. Technol.*, *7*, 121–140.

Hong, S.-Y., and J.-O. J. Lim (2006), The WRF single-moment 6-class microphysics scheme (WSM6), *J. Korean Meteorol. Soc.*, *42*, 129–151.

Kain, J. S., and J. M. Fritsch (1993), Convective parameterization for mesoscale models: The Kain-Fritsch scheme. The representation of cumulus convection in numerical models, *Meteorol. Monogr.*, *46*, 165–170.

Kain, J. S., S. J. Weiss, J. J. Levit, M. E. Baldwin, and D. R. Bright (2006), Examination of convection-allowing configurations of the WRF model for the prediction of severe convective weather: The SPC/NSSL spring program 2004, *Weather Forecast.*, *21*, 167–181.

Lock, A. P., A. R. Brown, M. R. Bush, G. M. Martin, and R. N. B. Smith (2000), A new boundary layer mixing scheme. Part I: Scheme description and single-column model tests, *Mon. Weather Rev.*, *128*, 3187–3199.

Louis, J.-F. (1979), A parametric model of vertical eddy fluxes in the atmosphere, *Boundary Layer Meteorol.*, *17*, 187–202.

Majewski, D., D. Liermann, P. Prohl, B. Ritter, M. Buchhold, T. Hanisch, G. Paul, and W. Wergen (2002), The operational global icosahedral-hexagonal gridpoint model GME: Description and high-resolution tests, *Mon. Weather Rev.*, *130*, 319–338.

May, P. T., J. H. Mather, G. Vaughan, C. Jakob, G. M. McFarquhar, K. N. Bower, and G. G. Mace (2008), The Tropical Warm Pool International Cloud Experiment, *Bull. Am. Meteorol. Soc.*, *89*, 629–645.

Mellor, G. L., and T. Yamada (1974), A hierarchy of turbulent closure models for planetary boundary layers, *J. Atmos. Sci.*, *31*, 1791–1806.

Mlawer, E. J., S. J. Taubman, P. D. Brown, M. J. Iacono, and S. A. Clough (1997), Radiative transfer for inhomogeneous atmospheres: RRTM, a validated k-correlated model for the longwave, *J. Geophys. Res.*, *102*, 16,663–16,682.

Morrison, H., G. Thompson, and V. Tatarskii (2009), Impact of cloud microphysics on the development of trailing stratiform precipitation in a simulated squall line: Comparison of one- and two-moment schemes, *Mon. Weather Rev.*, *137*, 991–1007.

Noh, Y., W. G. Cheon, S. Y. Hong, and S. Raasch (2003), Improvement of the K-profile model for the planetary boundary layer based on large eddy simulation data, *Boundary Layer Meteorol.*, *107*, 421–427.

Randall, D., M. Khairoutdinov, A. Arakawa, and W. Garbowski (2003), Breaking the cloud parameterization deadlock, *Bull. Am. Meteorol. Soc.*, *84*, 1547–1564.

Randall, D., et al. (2007), Climate models and their evaluation, in *Climate Change 2007: The Physical Science Basis. Contribution of Working Group I to the Fourth Assessment Report of the Intergovernmental Panel on Climate Change*, pp. 591–648, Cambridge Univ. Press, Cambridge, U. K.

Ritter, B., and J. F. Geleyn (1992), A comprehensive radiation scheme for numerical weather prediction models with potential applications in climate simulations, *Mon. Weather Rev.*, *119*, 342–367.

Smith, R. N. (1990), A scheme for predicting layer clouds and their water content in a general circulation model, *Q. J. R. Meteorol. Soc.*, *116*, 435–460.

Thompson, G., P. R. Field, R. M. Rasmussen, and W. D. Hall (2008), Explicit forecasts of winter precipitation using an improved bulk microphysics scheme. Part II: Implementation of a new snow parameterization, *Mon. Weather Rev.*, *136*, 5095–5115.

Tiedtke, M. (1989), A comprehensive mass flux scheme for cumulus parameterization in large scale models, *Mon. Weather Rev.*, *117*, 1779–1800.

Varble, A., A. M. Fridlind, E. J. Zipser, A. S. Ackerman, J.-P. Chaboureau, J. Fan, A. Hill, S. A. McFarlane, J.-P. Pinty, and B. Shipway (2011), Evaluation of cloud-resolving model intercomparison simulations using TWP-ICE observations: Precipitation and cloud structure, *J. Geophys. Res.*, *116*, D12206, doi:10.1029/2010JD015180.

Wang, Y., C. N. Long, L. R. Leung, J. Dudhia, S. A. McFarlane, J. H. Mather, S. J. Ghan, and X. Liu (2009), Evaluating regional cloud-permitting simulations of the WRF model for the Tropical Warm Pool International Cloud Experiment (TWP-ICE), Darwin, 2006, *J. Geophys. Res.*, *114*, D21203, doi:10.1029/2009JD012729.

Wapler, K., T. P. Lane, P. T. May, C. Jakob, M. J. Manton, and S. T. Siems (2010), Cloud-system-resolving model simulations of tropical cloud systems observed during the Tropical Warm Pool-International Cloud Experiment, *Mon. Weather Rev.*, *138*, 55–73, doi:10.1175/2009MWR2993.1.

Weisman, M. L., C. A. Davis, W. Wang, K. W. Manning, and J. B. Klemp (2008), Experiences with 0-36-h explicit convective forecasts with the WRF-ARW Model, *Weather Forecast.*, *23*, 407–437.

Wilson, D. R., and S. P. Ballard (1999), A microphysically based precipitation scheme for the UK Meteorological Office Unified Model, *Q. J. R. Meteorol. Soc.*, *125*, 1607–1636.

Xie, S., T. Hume, C. Jakob, S. Klein, R. McCoy, and M. Zhang (2010a), Observed large-scale structures and diabatic heating and drying profiles during TWP-ICE, *J. Clim.*, *23*, 57–79.

Xie, S., et al. (2010b), Clouds and More: ARM climate modeling best estimate data, *Bull. Am. Meteorol. Soc.*, *91*, 13–20.

Yang, G.-Y., and J. Slingo (2001), The diurnal cycle in the tropics, *Mon. Weather Rev.*, *129*, 784–801.

Zhang, M. H., J.-L. Lin, R. T. Cederwall, J. J. Yio, and S. C. Xie (2001), Objective analysis of ARM IOP data: Method and sensitivity, *Mon. Weather Rev.*, *129*, 295–311.

Zhu, P., B. A. Albrecht, V. P. Ghate, and Z.-D. Zhu (2010), Multiple scale simulations of stratocumulus clouds, *J. Geophys. Res.*, *115*, D23201, doi:10.1029/2010JD014400.